DOI: 10.1002/ ((please add manuscript number))
Article type: Full Paper

Enhancing Hydrogen Generation through Nanoconfinement of Sensitizers and Catalysts in a Homogeneous Supramolecular Organic Framework

Shang-Bo Yu,[a] Qi Qi,[a] Bo Yang,[a] Hui Wang,[a] Dan-Wei Zhang,[a] Yi Liu[b] and Zhan-Ting Li*[a]*

S.-B. Yu, Q. Qi, B. Yang, Dr. H. Wang, Prof. D.-W. Zhang, Prof. Z.-T. Li
Department of Chemistry, Shanghai Key Laboratory of Molecular Catalysis and Innovative Materials, and Collaborative Innovation Centre of Chemistry for Energy Materials (iChEM), Fudan University
2205 Songhu Road, Shanghai 200438, China
E-mail: ztli@fudan.edu.cn
Dr. Y. Liu
The Molecular Foundry, Lawrence Berkeley National Laboratory One Cyclotron Road
Berkeley, California 94720, USA
E-mail: yliu@lbl.gov

Keywords: supramolecular organic framework; nanoconfinement; photocatalysis; hydrogen evolution; cucurbit[8]uril

Enrichment of molecular photosensitizers and catalysts in a confined nanospace is conducive for photocatalytic reactions due to improved photo-excited electron transfer from photosensitizers to catalysts. Herein, we report the self-assembly of a highly stable three-dimensional (3D) supramolecular organic framework (**SOF-1**) from a rigid bipyridine-derived tetrahedral monomer and cucurbit[8]uril in water and its efficient and simultaneous intake of both $[Ru(bpy)_3]^{2+}$-based photosensitizers and various polyoxometalates (POMs) that can take place at very low loading. The enrichment substantially increases the apparent concentration of both photosensitizer and catalyst in the interior of the framework, which leads to a recyclable, homogeneous, visible light-driven photocatalytic system with 110-fold increase of the turnover number for the hydrogen evolution reaction.

1. Introduction

Photosensitized electron transfer catalysis has been utilized in a large number of photochemical reactions and solar-fuel applications.[1] Efficient electron transfer from

photosensitizers to catalysts requires their close proximity or contact. Increasing concentration is among the simplest methods for the enhancement of this process, which, however, may be economically unfavorable for practical use and may also suffer from the limitation of low solubility. In the past decades, several effective strategies have been developed for realizing this aim, which include covalent or non-covalent attachment of the two species into dyads or triads,[2] self-assembly into condensed entities through structural modifications,[3] and enrichment of either or both of the two species to the surface of a carrier or into a confined nanospace.[4,5] In the context of the enrichment strategy, most works have focused on the development of heterogeneous carriers. In contrast, examples of homogeneous enrichment are rare,[6,7] even though homogeneity can allow for maximum utilization of visible light irradiation as well as easy modulation of the relative ratio of the sensitizer, catalyst and substrate(s) to explore ideal conditions. We and others have recently developed a self-assembly strategy for the fabrication of homogeneous periodic supramolecular organic frameworks (SOFs),[8-11] including 3D diamondoid SOFs that can adsorb various organic guests.[8b-d] Herein we describe the self-assembly of a new highly stable supramolecular organic framework **SOF-1** from a new tetrahedral molecule with improved rigidity and cucurbit[8]uril (CB[8]) in water and its simultaneous adsorption for $[Ru(bpy)_3]^{2+}$-based photosensitizers and various polyoxametallate catalysts that can take place at very low concentrations in water. We further demonstrate that the nanoconfinement of the sensitizers and catalysts within the self-assembled framework leads to the construction of a new family of homogeneous, recyclable, visible-light-driven photocatalytic systems that exhibit remarkably enhanced efficiency for hydrogen evolution reactions (HERs).

2. Results and Discussion

The tetrahedral molecule **1** (**Figure 1**) was endowed more rigidity than the previously reported tetrapyridinium molecules by removing the methylene bridges.[8b-d] Despite the

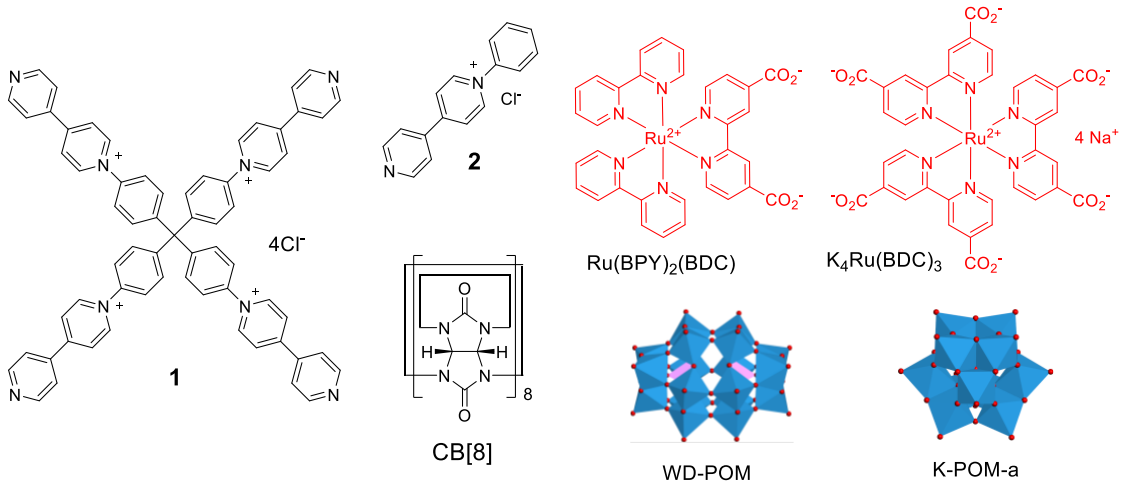

Figure 1. Structures of compound **1**, **2**, CB[8], photosensitizers ($[Ru(BDC)_3)]^{4-}$ (K^+ salt) and $Ru(BPY)_2(BDC)$) and POM catalysts (redox-active Wells-Dawson-type-$[P_2W_{18}O_{62}]^{6-}$ (K^+ salt, WD-POM) and Keggin-type $PW_{12}O_{40}^{3-}$ (Na^+ salt, K-POM-a)).

structural change, **1** displayed similar assembly behavior when mixing with CB[8] in water. **SOF-1** was assembled through the encapsulation of the heteromolecular bipyridyl dimers of **1** by CB[8].[12,13] The effective assembly was reflected by the remarkably improved solubility of CB[8], which itself has very low solubility in water (<0.01 mM).[14] When mixed with **1** in 2:1 ratio, the concentration of CB[8] could reach 4.0 mM, which corresponded to more than 400-fold increase of the solubility. This solubility is notably higher than that of previously reported SOFs formed by CB[8] and CH_2-bridged tetrahedral building blocks.[8b,11] ^{1}H NMR spectrum in D_2O showed that the resolution of the peaks of both components was reduced substantially due to complexation (Figure S1). 2D ^{1}H NMR diffusion ordered spectroscopy (DOSY) of their 1:2 ([**1**] = 1.0 mM) solution in D_2O showed that all the signals of the two compounds gave rise to a similar diffusion co-efficient (D) of 8.32×10^{-11} m^2/s (Figure S2), which was notably lower than that of **1** (1.91×10^{-10} m^2/s, Figure S3), supporting that **1** and CB[8] formed larger supramolecular entities. Dynamic light scattering (DLS) experiments revealed the formation of large aggregates in the 1:2 solution of **1** (1.0 mM) and CB[8] in water with a hydrodynamic diameter (D_H) of 43.82 nm. In contrast, the solution of **1** at 1.0 mM gave rise to a much smaller D_H of 2.328 nm (Figure S4). 1000-Fold dilution of the

mixture solution to [**1**] = 1.0 μM only led to marginal decrease of the D_H, suggesting that the large supramolecular entities remained aggregated even at such a low concentration (Figure S5). UV-vis titration experiments revealed an inflection point at [CB[8]]/[**1**] = ca. 2.0 when plotting the hypochromism at 314 nm and red-shifting of the absorption maximum of **1** against the concentration of CB[8] (Figures S6), which indicated an 1:2 stoichiometry. Using the method reported by Thordarson,[15] we determined the apparent binding constant (K_a) for the 1:2 complex formed between CB[8] and the bipyridyl units of **1** to be $2.1\times10_{16}$ M^{-2} (Figure S6d). The value was substantially higher than that of the 1:2 complex ($8.4 \times 10_{10}$ M^{-2}) formed between CB[8] and control **2** (Figure 1),[8a] indicating that significant positive cooperativity existed in **SOF-1**.

Solution-phase synchrotron small angle X-ray scattering (SAXS) profile for the above 1:2 solution ([**1**] = 2.0 mM) displayed a broad but clearly discernible peak with the *d*-spacing centered around 2.34 nm (Figure 2a). The peak matched well with the 111 facet (2.35 nm) of the simulated framework,[16] supporting the periodicity of **SOF-1** (Figure 3) in water. The synchrotron SAXS profiles of the polycrystals of **SOF-1**, which were obtained by slow evaporation of its aqueous solution at room temperature, exhibited five sharper scattering peaks at 2.78, 2.38, 1.86, 1.71, and 1.52 nm, respectively.[17] These peaks corresponded to the 110, 111, 200, 210, and 220 facets of the modelled structure of **SOF-1** (Figure 2b), which were also observed on the 2D profile (Figures 2e and 2f). These results supported that **SOF-1** also maintained the periodicity in the solid state. Thermogravimetric analysis showed that the solid-state **SOF-1** was stable up to 380 °C (Figure S7).

The modelled structure of **SOF-1**, including the chloride anions, has approximately 67% of void volume. The chair-styled pore defined by six cyclically-arranged CB[8] rings had a minimum aperture of approximately 2.3 nm (Figure 3). We then tested the adsorption ability of the ionic framework in water towards four different guests, including two photosensitizers

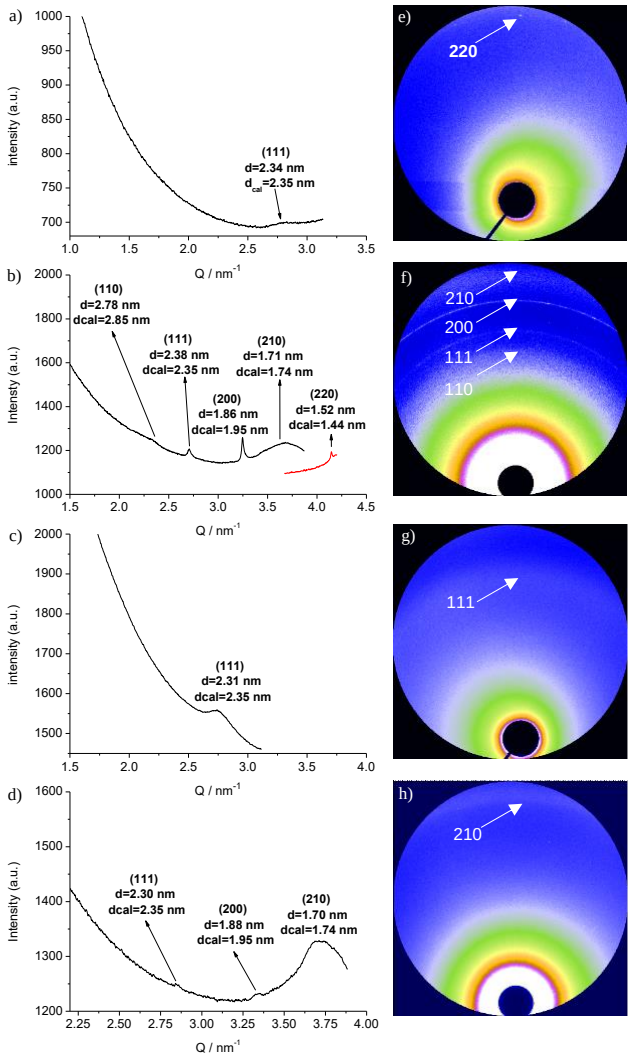

Figure 2. a) Solution-phase synchrotron SAXS profile of **SOF-1** ([**1**] = 2.0mM) in water, b) solid-phase synchrotron SAXS profile of **SOF-1** recorded separately for the same sample, and c) solid-phase synchrotron SAXS of **SOF-1** after adsorbing $K_4Ru(BDC)_3$ and WD-POM, d) solid-phase synchrotron SAXS of $K_4Ru(BDC)_3$/WD-POM@**SOF-1** after 10-time repeated irradiation (19 h); e) and f) 2D synchrotron SAXS corresponding to profile b; g) 2D synchrotron SAXS corresponding to profile c; h) 2D synchrotron SAXS corresponding to profile d.

($[Ru(BDC)_3]^{4-}$ (K^+ salt) and $Ru(BPY)_2(BDC)$) and two POM catalysts (redox-active Wells-Dawson-type-$[P_2W_{18}O_{62}]^{6-}$ (K^+ salt, WD-POM) and Keggin-type $PW_{12}O_{40}^{3-}$ (Na^+ salt, K-POM-a)) (Figure 1), by using the fluorescence spectroscopy. These two categories of guests have a size of 1.1-1.3 nm, and represent important components of integrated photocatalytic systems.[18] Both the Ru^{2+} complexes and the POMs quenched the fluorescence of **SOF-1**. The corresponding titration experiments indicated that maximum quenching was reached after 0.42, 0.70, 0.65, and 0.50 equivalent of the above-mentioned four anionic guests were added,

which corresponded to a relative ratio of 0.63, 0.35, 0.98 and 0.38 for their anion concentration over the concentration of **1** (5 μM) (Figure S8-S12). As expected, titration experiments also revealed that simultaneous addition of $K_4Ru(BDC)_3$ and WD-POM (10:1) into the solution of **SOF-1** also caused fluorescence quenching of **1** of **SOF-1** (Figure S13). Dialysis experiments using a membrane filter (1.0 kD molecular weight cutoff, shaken for 3 days) for the four adsorbed guests (30 μM) or their mixtures in **SOF-1** ([**1**] = 0.2 mM) indicated little guest diffusion into the outside water medium, as revealed by UV-vis spectroscopy (Figure S14-S17). The adsorption of $[Ru(BDC)_3]_{4-}$ and the POMs onto **SOF-1** can be explained by the exchange of hard base Cl^- of the framework with these soft guests to form soft (**SOF-1** and the guests) and hard ion (K^+ and Cl^-) pairs. For the neutral zwitterionic $Ru(BPY)_2(BDC)$, the effective adsorption may be due to similar soft ion pairing interactions between **1** and $Ru(BPY)_2(BDC)$ as well as increased hydrophobicity.

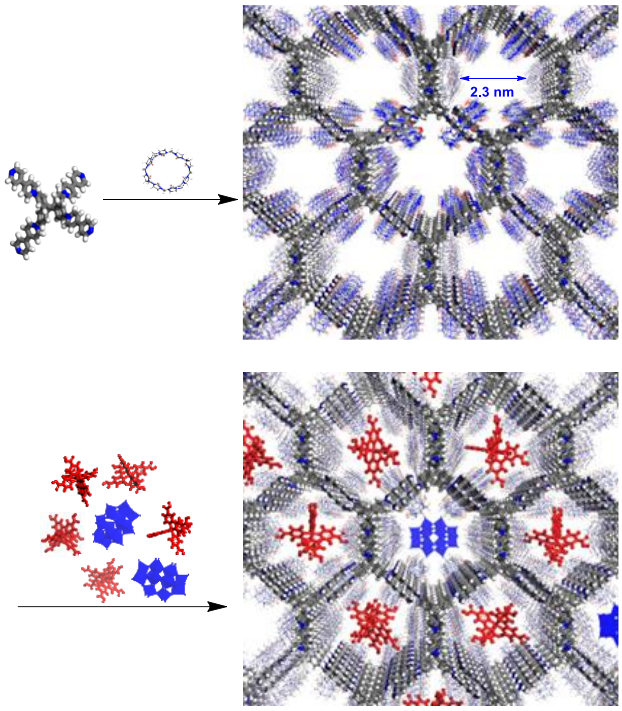

Figure 3. Illustration of the assembly of **1** and CB[8] into **SOF-1** in water and co-adsorption of Ru-photosensitizer (red) and polyoxometallate catalyst (blue).

On the basis of the observed high affinity of **SOF-1** towards all four guests, simultaneous adsorptions of both a photosensitizer and a catalyst were then investigated. Slow evaporation

of a mixture of **SOF-1**, WD-POM and either $[Ru(BDC)_3]^{4-}$ or $Ru(BPY)_2(BDC)$ afforded red or orange solid powders, which were thoroughly washed with water and methanol to remove non-adsorbed guests and then dried in vacuo at high temperature. TEM images showed that both samples formed uniform crystalline sheaf-like clusters, and energy dispersive X-ray (EDX) spectroscopy confirmed the existence of all the elements from both guests (Figure S18, S19). Synchrotron SAXS profiles of all four co-adsorbed samples based on different sensitizer/catalyst combinations, including $K_4Ru(BDC)_3$/WD-POM@**SOF-1**, $K_4Ru(BDC)_3$/K-POM-a@**SOF-1**, $Ru(BPY)_2(BDC)$/WD-POM@ **SOF-1**, and $Ru(BPY)_2(BDC)$ /K-POM-a@**SOF-1**, exhibited a clear peak centered at 2.31 nm, which corresponded to the 111 facet of the model framework (Figures 3c, 3g, and S20-S22). These results supported that **SOF-1** maintained its periodicity after absorbing the guests. DLS revealed a similar D_H of around 51 nm for all the above four mixtures (Figure S23). Further characterization by 2D DOSY showed that all observed signals possessed a comparable diffusion co-efficiency (Figure S24), which was similar to that of guest-free solution of **SOF-1**, again confirming the effective adsorption. Synchrotron SAXS profile of **SOF-1** that adsorbed only $K_4Ru(BDC)_3$ also showed that the framework maintained its periodicity (Figures S25).

Ru-pyridyl chromophores can be excited to Ru-pyridyl singlet and then transfers to the triplet, which returns to the ground state, leading to phosphorescence.[19] Steady-state and transient fluorescence spectra were then recorded to investigate the influence of **SOF-1** intake on the luminescence of $[Ru(BDC)_3]^{4-}$. It was expected that, in the absence of **SOF-1**, electrostatic repulsion would occur between anionic $[Ru(BDC)_3]^{4-}$ triplet and WD-POM to decrease electron transfer from the former to the latter, while the intake of **SOF-1** for both of them would lead to enhanced electron transfer from $[Ru(BDC)_3]^{4-}$ triplet to WD-POM. To address this speculation, luminescence quenching experiments were carried out. It was found that in the absence of **SOF-1**, adding anionic WD-POM (up to 6.98 μM) caused only slight quenching of the luminescence emission of $[Ru(BDC)_3]^{4-}$, with the dynamic quenching

constant (K_{SV}) being determined to be 8.51×10^3 l mol^{-1} (Figure S26) using the Stern-Volmer equation.[20] In contrast, in the presence of **SOF-1**, adding WD-POM (0-1.25 μM) could greatly reduce the luminescence emission of the $[Ru(BDC)_3]^{4-}$ (20 μM) triplet, and the K_{SV} was determined to be 1.214×10^6 l mol^{-1} (Figure S27). This value was 142-times higher than that of the above **SOF-1**-free system. The lifetime of the $[Ru(BDC)_3]^{4-}$ triplet exhibited dramatic decrease with the addition of WD-POM and finally stabilized at τ = 208 ns (excitation wavelength: 375 nm when 1.25 μM of WD-POM was added (Figure S28). The value was much smaller than that (430 ns) of the **SOF-1**-free system (Figure S29). Clearly, the intake of **SOF-1** could significantly promote electron transfer from excited $[Ru(BDC)_3]^{4-}$ to WD-POM (Figure S30).

The highest occupied molecular orbital (HOMO) energy of $[Ru(BDC)_3]^{4-}$ and $Ru(BPY)_2(BDC)$ and the lowest unoccupied molecular orbital (LUMO) energy of WD-POM and K-POM-a were determined to be –5.89, –5.81 and –4.78, –4.48 eV (Figure S31, Table S1), respectively.[7a,18] These energy levels aligned well with the water reduction potential. We then studied the HER efficiency using different photosensitizer/catalyst combinations in the presence and absence of **SOF-1**.

The maximum absorption of $[Ru(BDC)_3]^{4-}$ and $Ru(BPY)_2(BDC)$ appeared around 467 and 481 nm in the visible region, respectively (Figure S32). We thus chose visible light (>410 nm) as excitation for this study. HER was first conducted in acidic aqueous solution (pH = 1.8) using $[Ru(BDC)_3]^{4-}$–sensitized WD-POM as catalyst and methanol as sacrificial electron donor.[7a,18c,21] DLS experiments revealed that **SOF-1** exhibited a D_H of 42.93 nm in this acidic medium which was very close to that (43.82 nm) in neutral medium (Figure S4), supporting that **SOF-1** remained aggregated after the guest adsorption in this acidic solution.

HER experiments were then conducted by irradiating an aqueous solution (2 mL) for 19 hours in the presence of different amount of ($[Ru(BDC)_3]^{4-}$ and WD-POM, whose molar ratio

Table 1. Enhanced homogeneous and heterogeneous hydrogen evolution by different self-assemblies[a)]

Entry	[**1**] (μM) in **SOF-1**	Sensitizer (μM)	Catalyst (μM)	TON-S (with **SOF-1**)	TON-nS (no **SOF-1**)	TON-S/ TON-nS
1[b)]	50	$[Ru(BDC)_3]_4^-$ (1.80)	WD-POM (0.18)	1989	0[f)]	/
2[b)]	50	$[Ru(BDC)_3]_4^-$ (5.50)	WD-POM (0.55)	1929	18	110
3[b)]	50	$[Ru(BDC)_3]_4^-$ (9.10)	WD-POM (0.91)	1744	39	45
4[b)]	50	$[Ru(BDC)_3]_4^-$ (12.7)	WD-POM (1.27)	1376	38	36
5[b)]	50	$[Ru(BDC)_3]_4^-$ (16.4)	WD-POM (1.61)	1733	53	33
6[b,c)]	50	$[Ru(BDC)_3]_4^-$ (20.0)	WD-POM (2.00)	1775	50	36
7[b)]	50	$[Ru(BDC)_3]_4^-$ (24.5)	WD-POM (2.54)	1206	45	27
8[b)]	50	$[Ru(BDC)_3]_4^-$ (30.0)	WD-POM (3.00)	767	39	20
9[c)]	5	$[Ru(BDC)_3]_4^-$ (20.0)	WD-POM (2.00)	126	50	3
10[c)]	25	$[Ru(BDC)_3]_4^-$ (20.0)	WD-POM (0.18)	364	50	7
11[c)]	100	$[Ru(BDC)_3]_4^-$ (20.0)	WD-POM (2.00)	993	50	20
12[c)]	250	$[Ru(BDC)_3]_4^-$ (20.0)	WD-POM (2.00)	642	50	13
13	50	$[Ru(BDC)_3]_4^-$ (20.0)	K-POM-a (2.00)	3319	84	40
14	50	$Ru(BPY)_2(BDC)$ (20.0)	WD-POM (2.00)	1426	55	26
15	50	$Ru(BPY)_2(BDC)$ (20.0)	K-POM-a (2.00)	1477	52	29
16	50	$[Ru(BDC)_3]_4^-$ (20.0)	K-POM-b (2.00)	1574	53	30
17	50	$[Ru(BDC)_3]_4^-$ (20.0)	K-POM-c (2.00)	1700	66	26
18[d)]	50	$[Ru(BDC)_3]_4^-$ (20.0)	WD-POM (2.00)	1130	48	24
19[d)]	50	$Ru(BPY)_2(BDC)$ (20.0)	WD-POM (2.00)	753	40	19
20[d)]	50	$[Ru(BDC)_3]_4^-$ (20.0)	K-POM-a (2.00)	1088	51	21
21[d)]	50	$Ru(BPY)_2(BDC)$ (20.0)	K-POM-a (2.00)	874	43	20

[a)]Unless otherwise noted, the hydrogen evolution reaction were conducted under irradiation for 19 hours in the acid solution (pH = 1.8) that containing methanol (20 %, v/v) with the total volume 2.0 ml; [b)]The ratio of [sensitizer]/ [catalyst] was fixed at 10 (Entry 1-8); [c)]Varied concentrations of **SOF-1** (5, 25, 100 and 250 μM, respectively); [d)]Heterogeneous hydrogen evolution in acid solution (pH = 2.4) of MeCN and DMF (3:7, v/v) using triethanolamine (10%, v/v) as electron donor under 19 h irradiation; [e)]No detective hydrogen.

was kept at 10 (Table 1). In the absence of **SOF-1**, the generation of H_2 was observed at [WD-POM] ≥ 0.55 μM, and at [WD-POM] = 0.55 μM, turnover number (TON) was determined to be 18 (Entry 2，Table 1). In the presence of **SOF-1** ([**1**] = 50 μM), effective HER could be realized at [WD-POM] = 0.18 μM. Even at this low concentration, TON was still determined to be as high as 1989 (Entry 1, Table 1). This remarkably enhanced catalytic

activity clearly reflected the nanoconfinement effect of **SOF-1** for simultaneous enrichment of the photosensitizer and catalyst molecules. HERs were further conducted at higher concentrations of WD-POM while keeping the same photosensitizer/catalyst ratio (Entries 3-7, Table 1). For all the reactions, significant catalysis enhancement of **SOF-1** was observed, with up to 110-fold increase of TON (Entry 2, Table 1). Transient fluorescence spectra of these systems (Entries 1-7) showed that, with the simultaneous decrease of the concentrations of $[Ru(BDC)_3]^{4-}$ and WD-POM, the lifetime of the $[Ru(BDC)_3]^{4-}$ triplet also decreased from 292 ns to 115 ns, indicating enhanced electron transfer from the $[Ru(BDC)_3]^{4-}$ triplet to WD-POM as a result of simultaneous enrichment of them by **SOF-1** (Figure 4a).

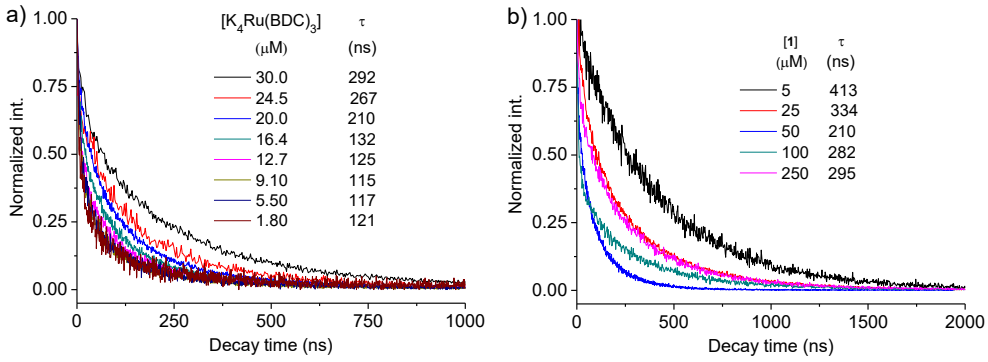

Figure 4. Transient fluorescence spectra of a) $K_4Ru(BDC)_3$ at different concentrations ([$(K_4Ru(BDC)_3$]/[WD-POM] = 10) in binary water-methanol (4:1, v/v, pH = 1.8 tuned by hydrochloric acid) solution containing **SOF-1** ([**1**] = 50 μM) and b) $K_4Ru(BDC)_3$ (20 μM) in the same binary solution in the presence of WD-POM (2 μM) and different concentration of **SOF-1**. The insets provide the fitted lifetimes (λ_{ex} = 375 nm, λ_{em} = 627 nm).

The influence of changing the loading of **SOF-1** was also studied by keeping the concentration of $[Ru(BDC)_3]^{4-}$ (20 μM) and WD-POM (2 μM) (Entries 6 and 9-12, Table 1). It can be found that, at all the tested concentrations, **SOF-1** promoted the generation of H_2. The highest enhancement was observed at [**1**] = 50 μM (Entry 6, Table 1). Transient fluorescence spectroscopy revealed the shortest lifetime (210 ns) for $[Ru(BDC)_3]^{4-}$ triplet at this concentration of **1** (Figure 4b), which again indicated the fastest electron transfer at this concentration.

The enhancement of **SOF-1** for the photocatalytic H_2 production of different combinations of the sensitizers and catalysts was also investigated at the identical sensitizer (20 μM)/catalyst (2 μM) ratio of 10 and the concentration of **SOF-1** ([**1**] = 50 μM). 40-, 26-, and 29-Fold increases were observed for the combinations of $[Ru(BDC)_3]^{4-}$/K-POM-a, $Ru(BPY)_2(BDC)$/WD-POM and $Ru(BPY)_2(BDC)$/K-POM-a (Entries 13-15, Table 1). Other Keggin-type POMs, such as K-POM-b ($H_3SiW_{12}O_{40}$) and K-POM-c ($H_3PMo_{12}O_{40}$), were also tested with $[Ru(BDC)_3]^{4-}$ (20 μM) as the photosensitizer in the solution of **SOF-1** ([1] = 50 μM). At [K-POM-b] = [K-POM-c] = 2 μM, 30- and 26-fold increases of the TONs were observed (Table 1, Entry 16 and 17).

Under the above catalytic conditions ([**1**] in **SOF-1** = 50 μM, $[[Ru(BDC)_3]^{4-}]$ = 20 μM, and [WD-POM] = 2.0 μM), H_2 generation could last for about 100 hours (Figure S33a). After this time point, further irradiation caused no observable H_2 generation. However, after being left to stand for, typically, 12 hours, irradiating the solution could lead to the generation of H_2 again. The process could be repeated at least for 10 times. In contrast, in the absence of **SOF-1**, the irradiation-induced generation of H_2 could last for only about 30 hours (Figure S33b). Moreover, irradiating this solution again did not lead to detectable H_2 generation. The ratios of the TON values of the above recycling catalysis in the presence of **SOF-1** over this **SOF-1**-free system are provided in Figure 5. After 10 times of recycling, TON was still as 26-fold high as that of the **SOF-1**-free system, reflecting the substantially increased stability of both $[Ru(BDC)_3]^{4-}$ and WD-POM after being loaded within **SOF-1**.[22] The absorption spectrum of the solution after 10 times of recycling was also recorded, which revealed about 27% of decrease for the absorption of $K_4Ru(BDC)_3$ (at 467 nm). This decrease was reasonably consistent with the decrease extent of the enhancement effect (about 25%) of the catalytic system after recycling for 10 times (Figure S34), which might be attributed to partial decomposition of the photosensitizer as reported for other photocatalytic systems.[23] DLS for

the solution after 10 times of recycling afforded a D_H (58.77 nm) which was comparable to that of the originally prepared sample (50.75 nm) (Figure S23), supporting that **SOF-1** still maintained its integrity after repeated use. The synchrotron SAXS profile of the solid sample obtained by evaporation of the solution exhibited three scattering peaks at 2.30, 1.88 and 1.70 nm (Figure 3d, 3h), respectively. These peaks corresponded to the 111, 200, and 220 facets of **SOF-1**, also supporting that **SOF-1** kept its regularity after repeated use. When the reaction was carried out heterogeneously in a mixture of acetonitrile and *N*,*N*-dimethyl formamide (3:7 v/v) with WD-POM or K-POM-a as catalyst and triethanolamine as sacrificial electron donor, the HER efficiency was found to increase by 19 to 24 times (Entries 18-21, Table 1), demonstrating that the porous feature of **SOF-1** could provide more accessible surfaces for protons and sacrificial electron donors.[8c]

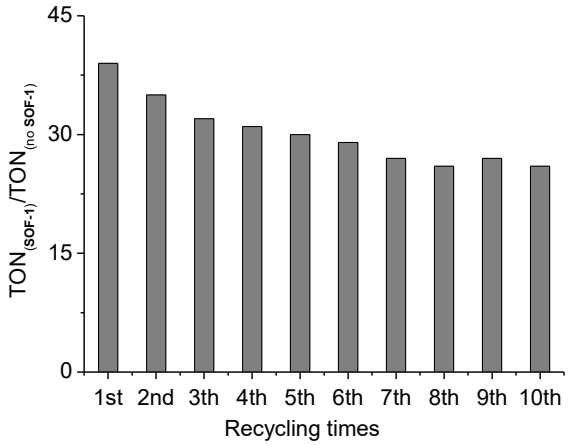

Figure 5. Ratio of TON values in the presence and absence of **SOF-1** ([**1**] = 50 μM) versus the recycling times in binary water-methanol (20 %, v/v) (pH = 1.8, $[[Ru(BDC)_3]_4^-]$ = 20 μM, [WD-POM] = 2 μM), irradiation time = 19 hours).

3. Conclusion

In summary, we have developed a new strategy for improving the efficiency of electron transfer between photosensitizer and catalyst molecules and consequently HER catalytic activities by using a new supramolecular organic framework for nanoconfinement through the co-adsorption of photosensitizer and catalyst molecules. The robust intake of the framework for both photosensitizer and catalyst molecules leads to remarkable their enrichment even at

very low loading. The high stability of the framework allows for long-time irradiation of the resulting integrated catalytic systems and their recyclable use while maintaining high catalytic efficiency. We believe that our method represents a new general approach of nanoconfinement, which may be readily extended to other photocatalytic processes such as oxygen evolution reaction and CO_2 reduction.

Supporting Information
Supporting Information is available from the Wiley Online Library or from the author.

4. Acknowledgements

We thank NSFC (Nos. 91227108, 21432004, and 21529201) for financial support, Shanghai Synchrotron Radiation Facility for providing BL16B1 and BL14B1 beamlines for collecting the synchrotron X-ray scattering and diffraction data, and the SIBYLS Beam-line 12.3.1 of the Advanced Light Source, Lawrence Berkeley National Laboratory, for collecting solution-phase synchrotron small-angle X-ray scattering data. YL thanks the support from the Molecular Foundry, Law-rence Berkeley National Laboratory, supported by the Office of Science, Office of Basic Energy Sciences, Scientific User Facilities Division, of the U.S. Department of Energy under Contract No. DE-AC02- 05CH11231.

Received: ((will be filled in by the editorial staff))
Revised: ((will be filled in by the editorial staff))
Published online: ((will be filled in by the editorial staff))

References

[1] a) F. Wen, C. Li, *Acc. Chem. Res.* **2013**, *46*, 2355; b) G. Xie, K. Zhang, B. Guo, Q. Liu, L. Fang, J. R. Gong, *Adv. Mater.* **2013**, *25*, 3820; c) W. Tu, Y. Zhou, Z. Zou, *Adv. Mater.* **2014**, *26*, 4607; d) H.-Q. Peng, L.-Y. Niu, Y.-Z. Chen, L.-Z. Wu, C.-H. Tung, Q.-Z. Yang, *Chem. Rev.* **2015**, *11*, 7502; e) S.-J. Jeon, T.-W. Kang, J.-M. Ju, M.-J. Kim, J. H. Park, F. Raza, J. Han, H.-R. Lee, J.-H. Kim, *Adv. Funct. Mater.* **2016**, *26*, 8211; f) M. Jakesova, D. H. Apaydin, M. Sytnyk, K. Oppelt, W. Heiss, N. S. Sariciftci, E. D. Glowacki, *Adv. Funct. Mater.* **2016**, *26*, 5247; g) Q. Liu, L.-Z. Wu, *Natl. Sci. Rev.* **2017**, *4*, 359.

[2] a) S. Fukuzumi, K. Ohkubo, T. Suenobu, *Acc. Chem. Res.* **2014**, *47*, 1455; b) J. M. Sumliner, H. Lü, J. Fielden, Y. V. Geletii, C. L. Hill, *Eur. J. Inorg. Chem.* **2014**, 635; c) G. Rotas, K. Stranius, N. Tkachenko, N. Tagmatarchis, *Adv. Funct. Mater.* **2018**, *28*, 1702278.

[3] a) L.-Z. Wu, B. Chen, Z.-J. Li, C.-H. Tung, *Acc. Chem. Res.* **2014**, *47*, 2177; b) T. H. Noh, O.-S. Jung, *Acc. Chem. Res.* **2016**, *49*, 1835; c) J. Willkomm, K. L. Orchard, A. Reynal, E. Pastor, J. R. Durrant, E. Reisner, *Chem. Soc. Rev.* **2016**, *45*, 9; d) L. Zang, *Acc. Chem. Res.* **2015**, *48*, 2705; e) P. Hu, L. Chen, X. Kang, S. Chen, *Acc. Chem. Res.* **2016**, *49*, 2251; f) S. Bhattacharya, S. K. Samanta, *Chem. Rev.* **2016**, *116*,11967.

[4] a) B. Wang, X. Wang, *Small* **2015**, *11*, 3097; b) J.-L. Wang, C. Wang, W. Lin, *ACS Catal.* **2012**, *2*, 2630; c) Y. Fu, D. Sun, Y. Chen, R. Huang, Z. Ding, X. Fu , Z. Li , *Angew. Chem. Int. Ed.* **2012**, *51*, 3364; d) S. L. Li, Q. Xu, *Energy Environ. Sci.* **2013**, *6*, 1656; e) S. Wang, W. Yao, J. Lin, Z. Ding, X. Wang, *Angew. Chem. Int. Ed.* **2014**, *53*, 1034; f) T. Zhang, W. Lin, *Chem. Soc. Rev.* **2014**, *43*, 5982; g) N. M. Julkapli, S. Bagheri, *Int. J. Hydrogen Energ.* **2015**, *40*, 948; h) M. Hansen, F. Li, L. Sun, B. König, *Chem. Sci.* **2014**, *5*, 268.

[5] a) L.-M. Zhao, Q.-Y. Meng, X.-B. Fan, C. Ye, X.-B. Li, B. Chen, V. Ramamurthy, C.-H. Tung, L.-Z. Wu, *Angew. Chem. Int. Ed.* **2017**, *56*, 3020; b) R. Wang, K.-Q. Lu, Z.-R. Tang, Y.-J. Xu, *J. Mater. Chem. A* **2017**, *5*, 3717; c) A. Kruth, A. Quade, V. Brüser, K.-D. Weltmann, *J. Phys. Chem. C* **2013**, *117*, 3804; d) X.-H. Li, J. Zhang, X. Chen, A. Fischer, A. Thomas, M. Antonietti, X. Wang, *Chem. Mater.* **2011**, *23*, 4344; e) A. Greer, *Nature* **2007**, *447*, 273; f) N. Alarcos, B. Cohen, M. Ziółek, A. Douhal, *Chem. Rev.* **2017**, *117*, 13639.

[6] a) J.-X. Jian, Q. Liu, Z.-J. Li, F. Wang, X.-B. Li, C.-B. Li, B. Liu, Q.-Y. Meng, B. Chen, K. Feng, C.-H. Tung, L.-Z. Wu, *Nat. Commun.* **2013**, *4*, 2695; b) W.-J. Liang, F. Wang, M. Wen, J.-X. Jian, X.-Z. Wang, B. Chen, C.-H. Tung, L.-Z. Wu, *Chem. Eur. J.* **2015**, *21*, 3187.

[7] a) J. Tian, Z.-Y. Xu, D.-W. Zhang, H. Wang, S.-H. Xie, D.-W. Xu, Y.-H. Ren, H. Wang, Y. Liu, Z.-T. Li, *Nat. Commun.* **2016**, *7*, 11580; b) S. Frühbeißer, G. Mariani, F. Gröhn, *Polymers* **2016**, *8*, 180.

[8] a) K.-D. Zhang, J. Tian, D. Hanifi, Y. Zhang, A. C.-H. Sue, T.-Y. Zhou, L. Zhang, X. Zhao, Y. Liu, Z.-T. Li, *J. Am. Chem. Soc.* **2013**, *135*, 17913; b) J. Tian, T.-Y. Zhou, S.-C. Zhang, S. Aloni, M. V. Altoe, S.-H. Xie, H. Wang, D.-W. Zhang, X. Zhao, Y. Liu, Z.-T. Li,

Nat. Commun. **2014**, *5*, 5574; c) J. Tian, C. Yao, W.-L. Yang, L. Zhang, D.-W. Zhang, H. Wang, F. Zhang, Y. Liu, Z.-T. Li, Chin. Chem. Lett. 2017, 28, 798; d) Y.-P. Wu, B. Yang, J. Tian, S.-B. Yu, H. Wang, D.-W. Zhang, Y. Liu, Z.-T. Li, *Chem. Commun.* **2017**, *53*, 13367.

[9] M. Pfeffermann, R. Dong, R. Graf, W. Zajaczkowski, T. Gorelik, W. Pisula, A. Narita, K. Müllen, X. Feng, *J. Am. Chem. Soc.* **2015**, *137*, 14525.

[10] Y. Zhang, T.-G. Zhan, T.-Y. Zhou, Q.-Y. Qi, X.-N. Xu, X. Zhao, *Chem. Commun.* **2016**, *52*, 7588.

[11] Y. Li, Y. Dong, X. Miao, Y. Ren, B. Zhang, P. Wang, Y. Yu, B. Li, L. Isaacs, L. Cao, *Angew. Chem. Int. Ed.* **2018**, 57, 729.

[12] a) Y. H. Ko, E. Kim, I. Hwang, K. Kim, *Chem. Commun.* **2007**, *13*, 1305; b) Y. H. Ko, I. Hwang, D.-W. Lee, K. Kim, *Israel J. Chem.* **2011**, *51*, 506; c) Y. Liu, H. Yang, Z. Wang, X. Zhang, Chem. Asian J. 2013, 8, 1626; d) Y. Zhang, T.-Y. Zhou, K.-D. Zhang, J.-L. Dai, Y.-Y. Zhu, X. Zhao, *Chem. Asian J.* **2014**, *9*, 1530; e) L. Isaacs, *Acc. Chem. Res.* **2014**, *47*, 2052; f) J. Tian, L. Zhang, H. Wang, D.-W. Zhang, Z.-T. Li, *Supramol. Chem.* **2016**, *28*, 769.

[13] a) G. Bergamini, A. Fermi, M. Marchini, M. Locritani, A. Credi, M. Venturi, F. Negri, P. Ceroni, M. Baroncini, *Chem. Eur. J.* **2014**, *20*, 7054; b) R. M. Parker, J. Zhang, Y. Zheng, R. J. Coulston, C. A. Smith, A. R. Salmon, Z. Yu, O. A. Scherman, C. Abell, *Adv. Funct. Mater.* **2015**, *25*, 4091.

[14] J. Lagona, P. Mukhopadhyay, S. Chakrabarti, L. Isaacs, *Angew. Chem. Int. Ed.* **2005**, 44, 4844; b) S. J. Barrow, S. Kasera, M. J. Rowland, J. del Barrio, O. A. Scherman, *Chem. Rev.* **2015**, *115*, 12320.

[15] P. Thordarson, *Chem. Soc. Rev.* **2011**, *40*, 1305.

[16] Accelrys Materials Studio Release Notes, Release 7.0, Accelrys Software Inc., San Diego, USA.

[17] a) J. Zeng, F. Bian, J. Wang, X. Li, Y. Wang, F. Tian, P. Zhou, *J. Synchrotron Rad.* **2017**, *24*, 509; b) T.-Y. Yang, W. Wen, G.-Z. Yin, X.-L. L, M. Gao, Y.-L. Gu, L. Li, Y. Liu, H. Lin,

X.-M. Zhang, B. Zhao, T.-K. Liu, Y.-G. Yang, Z. Li, X.-T. Zhou, X.-Y. Gao, *Nucl. Sci. Tech.* **2015**, *26*, 020101.

[18] a) J. J. Walsh, A. M. Bond, R. J. Forster, T. E. Keyes, *Coord. Chem. Rev.* **2016**, *306*, 217; b) H. Lv, J. Song, H. Zhu, Y. V. Geletii, J. Bacsa, C. Zhao, T. Lian, D. G. Musaev, C. L. Hill, *J. Catal.* **2013**, *307*, 48; c) Z.-M. Zhang, T. Zhang, C. Wang, Z. Lin, L.-S. Long, W. Lin, *J. Am. Chem. Soc.* **2015**, *137*, 3197; d) K. Kumamoto, K. Tsuchibashi, A. D. Pramata, M. Yuasa, K. Shimanoe, T. Kida, *J. Phys. Chem. C* **2017**, *121*, 13515; e) K. A. Opperman, S. L. Mecklenburg, T. J. Meyer, *Inorg. Chem.* **1994**, *33*, 5295; f) H. Sun, M. Z. Hoffman, Q. G. Mulazzani, *Res. Chem. lntermed.* **1994**, *320*, 735; g) V. M. Hultgren, A. M. Bond, A. G. Wedd, *J. Chem. Soc. Dalton Trans.* **2001**, 1076; h) S. Tanaka, M. Annaka, K. Sakai, *Chem. Commun.* **2012**, *48*, 1653; i) Y. V. Geletii, Z. Huang, Y. Hou, D. G. Musaev, T. Lian, C. L. Hill, *J. Am. Chem. Soc.* **2009**, *131*, 7522.

[19] a) J. J. Concepcion, J. W. Jurss, M. K. Brennaman, P.G. Hoertz, A. O. T. Patrocinio, N. Y. M. Iha, J. L. Templeton, T. J. Meyer, *Acc. Chem. Res.* **2009**, *42*, 1954; b) J. V. Casper, T. J. Meyer, *J. Am. Chem. Soc.* **1983**, *105*, 5583.

[20] I. A. Weinstock, *Chem. Rev.* **1998**, *98*, 113.

[21] a) T. Rüther, V. M. Hultgren, B.P. Timko, A. M. Bond, W. R. Jackson, A. G. Wedd, *J. Am. Chem. Soc.* **2003**, *125*, 10133; b) T. Yamase, X. Cao, S. Yazaki, *J. Mol. Catal. A: Chem.* **2007**, *262*, 119; c) Z. Zhang, Q. Lin, S.-T. Zheng, X. Bu, P. Feng, *Chem. Commun.* **2011**, *47*, 3918; d) T. Yamase, N. Takabanashi, M. Kaji, *J. Chem. Soc. Dalton Trans.* **1984**, 793; e) W.-C. Chen, C. Qin, X.-L. Wang, K-Z. Shao, Z.-M. Su, E.-B. Wang, *Cryst. Growth Des.* **2016**, *16*, 2481; f) Z. Y. Zhang, Q. P. Lin, D. Kurunthu, T. Wu, F. Zuo, S. T. Zheng, C. J. Bardeen, X. H. Bu, P. Y. Feng, *J. Am. Chem. Soc.* **2011**,*133*, 6934; g) S. J. Li, S. M. Liu, S. X. Liu, Y. W. Liu, Q. Tang, Z. Shi, S. X. Ouyang, J. H. Ye, *J. Am. Chem. Soc.* **2012**, *134*, 19716.

[22] a) D. Astruc, F. Lu, J. R. Aranzaes, *Angew. Chem. Int. Ed.* **2005**, *44*, 7852; b) K. Mori, T. Hara, T. Mizugaki, K. Ebitani, K. Kaneda, *J. Am. Chem. Soc.* **2004**, *126*, 10657; c) W. Gan, P.

J. Dyson, G. Laurenczy, *ChemCatChem*, **2013**, *5*, 3124; d) L. E. Heim, N. E. Schlöer, J.-H. Choi, M. H. G. Prechtl, *Nat. Commun.* **2014**, *5*, 3621; e) J. F. Hull, Y. Himeda, W.-H. Wang, B. Hashiguchi, R. Periana, D. J. Szalda, J. T. Muckerman, E. Fujita, *Nat. Chem.* **2012**, *4*, 383; f) G. P. M. van Klink, H. P. Dijkstra, G. van Koten, *C. R. Chimie*, **2003**, *6*, 1079.

[23] a) R. Grünwald, H. Tributsch, *J. Phys. Chem.* **1997**, *101*, 2564; b) S. Shalini, R. Balasundaraprabhu, T. S. Kumar, N. Prabavathy, S. Senthilarasu, S. Prasanna, *Int. J. Energy Res.* **2016**, *40*, 1303; c) M. Kirch, J. M. Lehn, J. P. Sauvage, *Helv. Chim. Acta* **1979**, *62*, 1345; d) H. A. F. Wemer, R. Bauer, *J. Mol. Catal.*, **1994**, *88*, 185; e) C. Königstein, *J. Photoch. Photobio. A*, **1995**, *90*, 141; f) N. L. Fry, P. K. Mascharak, *Acc. Chem. Res.*, **2011**, *44*, 289; g) P. Comte, M. K. Nazeeruddin, F. P. Rotzinger, A. J. Frank, M. Grätzel, *J. Mol. Catal.* **1989**, *52*, 63; h) P. K. Ghosh, B. S. Brunschwig, M. Chou, C. Creutz, N. Sutin, *J. Am. Chem. Soc.* **1984**, *106*, 4772; i) M. Hara, C. C. Waraksa, J. T. Lean, B. A. Lewis, T. E. Mallouk, *J. Phys. Chem. A* **2000**, *104*, 5275; j) M. D. Kärkäs, O. Verho, E. V. Johnston, B. Åkermark, *Chem. Rev.* **2014**, *114*, 11863; k) B. Limburg, E. Bouwman, S. Bonnet, *ACS Catal.* **2016**, 5273.

The table of contents entry

Enhanced H_2 generation by SOF intake for both photosensitizer and catalyst in solution: Electrostatic interaction drives a water-soluble supramolecular organic framework as nanoconfinement to intake both Ru^{2+} photosensitizers and polyoxometallate catalysts of very low concentrations, leading to remarkable promotion of electron transfer from excited sensitizers to catalysts that allows for visible-light-induced homogeneous reduction of proton into hydrogen in recyclable manner.

Keyword
supramolecular organic framework, nanoconfinement, photocatalysis, hydrogen evolution, cucurbit[8]uril

Shang-Bo Yu, Qi Qi,[a] Bo Yang, Hui Wang, Dan-Wei Zhang,[a] Yi Liu,*[b] Zhan-Ting Li*[a]

Enhancing Hydrogen Generation through Nanoconfinement of Sensitizers and Catalysts in a Homogeneous Supramolecular Organic Framework

ToC figure

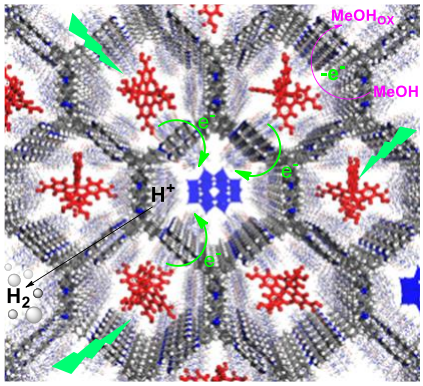

Supporting Information

Enhancing Hydrogen Generation through Nanoconfinement of Sensitizers and Catalysts in a Homogeneous Supramolecular Organic Framework

Shang-Bo Yu, Qi Qi, Bo Yang, Hui Wang, Dan-Wei Zhang, Yi Liu, and Zhan-Ting Li**

Materials: All reagents were obtained from commercial suppliers and used without further purification unless otherwise noted. All reactions were carried out under a dry nitrogen atmosphere. All solvents were dried before use following standard procedures.

Characterization: ^{1}H NMR spectra were recorded with a 400 MHz spectrometer. ^{1}H NMR diffusion-ordered spectroscopic spectra were recorded with a 400 / 500 MHz spectrometer in the indicated solvents at 25 °C. ^{1}H NMR diffusion-ordered spectroscopic experiments were carried out with a 400 NMR spectrometer. Solid-phase or solution-phase synchrotron X-ray-scattering experiments were performed on the BL16B beamline of Shanghai Synchrotron Radiation Facility, using a fixed wavelength of 0.124 nm, a sample-to-detector distance of 1.84 m and an exposure time of 2000 s. The 2D scattering pattern was collected on a charge-coupled device camera, and the curve intensities versus q were obtained by integrating the data from the pattern. Scanning electron micrographs of the samples were obtained on a Nova nano SEM 450 Field Emission Scanning Electron Microscope at 3.00 kV with the material adhered to the SEM sample holder directly or on a Phenom China Scanning Electron Microscope at 15.00 kV after the material that adhered to the sample holder was been gilded to 10^{-1}-10^{-2} vacuum degree. Transmission electron micrographs were recorded on a JEM 2011 FETEM microscope at 200 kV aligned for low dose (10 e Å^{-2} s^{-1}) diffractive imaging. TGA experiments were performed on a Model TGA/SDTA 851 instrument. Samples were placed in alumina pans and heated at a rate of 5 °C per minute from 100 to 900 °C under a nitrogen atmosphere. UV-Vis spectra were performed on a Perkin-Elmer 750s instrument from 200-800 nm at the scan rate of 3 nm/ internal. DLS experiments were performed on a Malvern Zetasizer Nano ZS90 light scattering Instrument. Fluorescence measurements were performed on a VARIAN CARY Eclipse Fluorescence Spectrophotometer and PerkinElmer LS 55 Luminescence spectrometer. Visible FL spectra (steady-state and transient luminescence spectra) were recorded on Edinburgh Fluorescence Spectrometer FLS980 instrument with Xenon lamp (370 nm) as excitation source. H_2 was characterized by GC-2010 using helium as the carrier gas with a BDI plasma detector.

Table S1. Molecular orbital energy of the guests (photosensitizers and catalysts).

Compound	λ_{max} (nm)[a]		$\varepsilon\ \lambda_{max}$ ($M^{-1}\ cm^{-1}$)	E_g[b] (eV)	E_{red}[c] (eV)	E_{ox}[c] (eV)	HOMO[d] (eV)	LUMO[d] (eV)
	LC	MLCT						
$Ru(BPY)_2(BDC)$	284	481	7539	2.16[2]	/	1.31[2]	-5.81	-3.65
$K_4Ru(BDC)_3$	301	467	17 518	2.20[2]	/	1.39[2]	-5.89	-3.69
WD-POM	/	/	48 525	3.44[3]	0.28[3]	/	-8.22[3]	-4.78[3]
K-POM-a	/	/	34 402	3.59	-0.02[4]	/	-8.39	-4.48
K-POM-b	/	/	38 605	3.31	-0.19[4]	/	-7.79	-4.48
K-POM-c	/	/	64 765	3.30	0.32[5]	/	-8.12	-4.82

[a] Measured in water.

[b] The optical band gap E_g=1240 / λ_{onset} was estimated from the tangents of the absorption edges of their UV/Vis spectra (Figure S25), nearly same the reported literature.[2-5]

[c] Potentials versus normal hydrogen electrode (NHE).[2-5]

[d] HOMO and LUMO energies were calculated with reference to NHE (4.50 eV), LUMO = -(4.50 + E_{red}); HOMO = -(4.50 + E_{ox}); HOMO = LUMO − E_g .

LC: Ligand-centered (LC, π→π*) transition band.

MLCT: Metal-to ligand charge transfer (MLCT, d→π*) band.

Compound $K_4Ru(BDC)_3$ was synthesized as the previous reported literature.[6, 7] Compound $Ru(BPY)_2(BDC)$ was synthesized as the previous reported literature.[8]

The fitting of apparent associate constant for SOF

The fitting of apparent associate constant for **SOF-1** composed of **1** and CB[8] was conducted with the help of the software MATLAB R2017a. The UV-Vis change up on titration with a 2:1 host-guest system was utilized to fit the stoichiometry ratio using the program "uv2to1bb" (Equation 1). Carefully fitting of 'Enter factor to change htot (usually 1)', 'Number of iteration to perform (ca. 200-1000)', 'Enter guess for binding constant (s)' and 'Enter guess for DeltaXX' was done to final 'stable' results.

Equation 1:

$$\Delta A_{obs} = \frac{\varepsilon_{\Delta HG}[G]_0 K_1[\mathrm{H}] + 2\varepsilon_{\Delta H2G}[G]_0 K_1 K_2[H]^2}{1 + K_1[\mathrm{H}] + K_1 K_2[H]^2}$$

References

[1] S.-B. Yu, H. Lyu, J. Tian, H. Wang, D.-W. Zhang, Y. Liu, Z.-T. Li, *Polym. Chem.* **2016**, *7* , 3392.

[2] H. Park, E. Bae, J.-J. Lee, J. Park, W. Choi, *J. Phys. Chem. B* **2006**, *110*, 8740.

[3] J. Tian, Z.-Y. Xu, D.-W. Zhang, H. Wang, S.-H. Xie, D.-W. Xu, Y.-H. Ren, H. Wang, Y. Liu, Z.-T. Li, *Nat. Commun.* **2016**, *7*, 11580.

[4] M. T. Pope, G. M. Varga jr., *Inorg. Chem.* **1966**, *5*, 1249.

[5] J.-Y. Niu, M.-L. Wei, J.-P. Wang, D.-B. Dang, *Eur. J. Inorg. Chem.* **2004**, *160*, 170.

[6] M. Schwalbe, B. Schäfer, H. Görls, S. Rau, S. Tschierlei, M. Schmitt, J. Popp, G. Vaughan, W. Henry, J. G. Vos, *Eur. J. Inorg. Chem.* **2008**, 3310.

[7] X. Su, L. Guo, Y. Ma, X. Li, *Spectrochim. Acta A* **2016**, *152*, 468.

[8] H. Xia, Y. Zhu, D. Lu, M. Li, C. Zhang, B. Yang, Y. Ma, *J. Phys. Chem. B* **2006**, *110*, 18718.

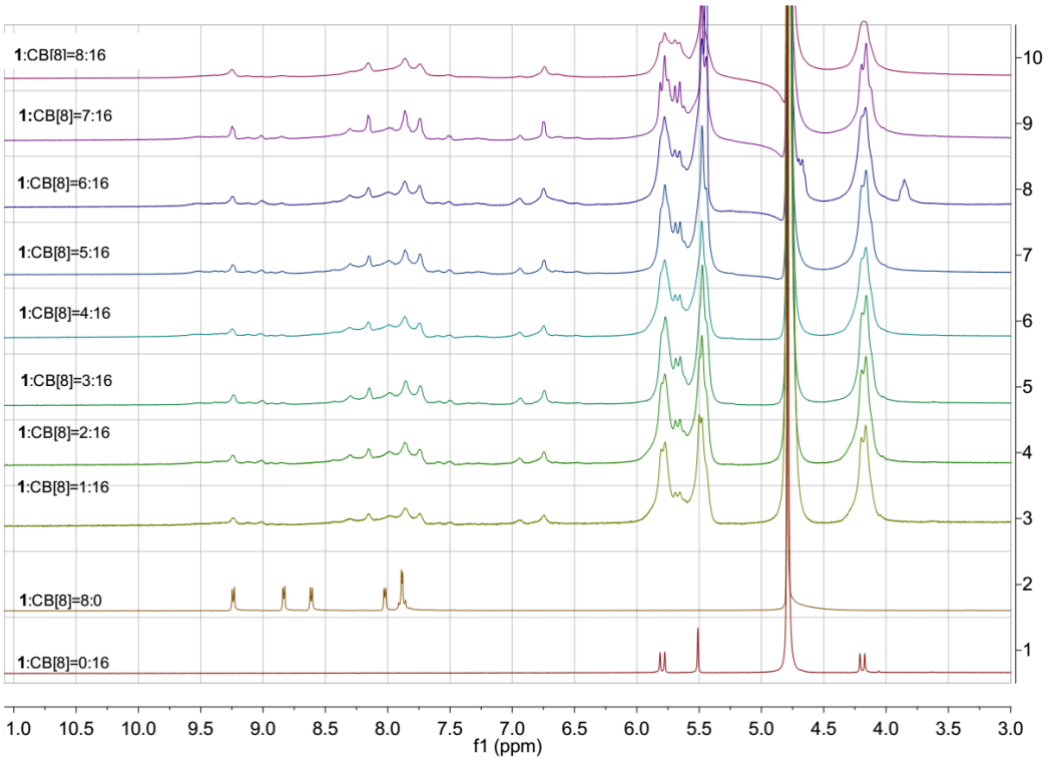

Figure S1. The ^{1}H NMR of gradually dissolvation of CB[8] in D_2O with increasing amounts of molecule **1** (400 MHz, 25 °C, [CB[8]] = 2.0 mM). When 0.5 equiv. **1** added, the CB[8] dissolved completely.

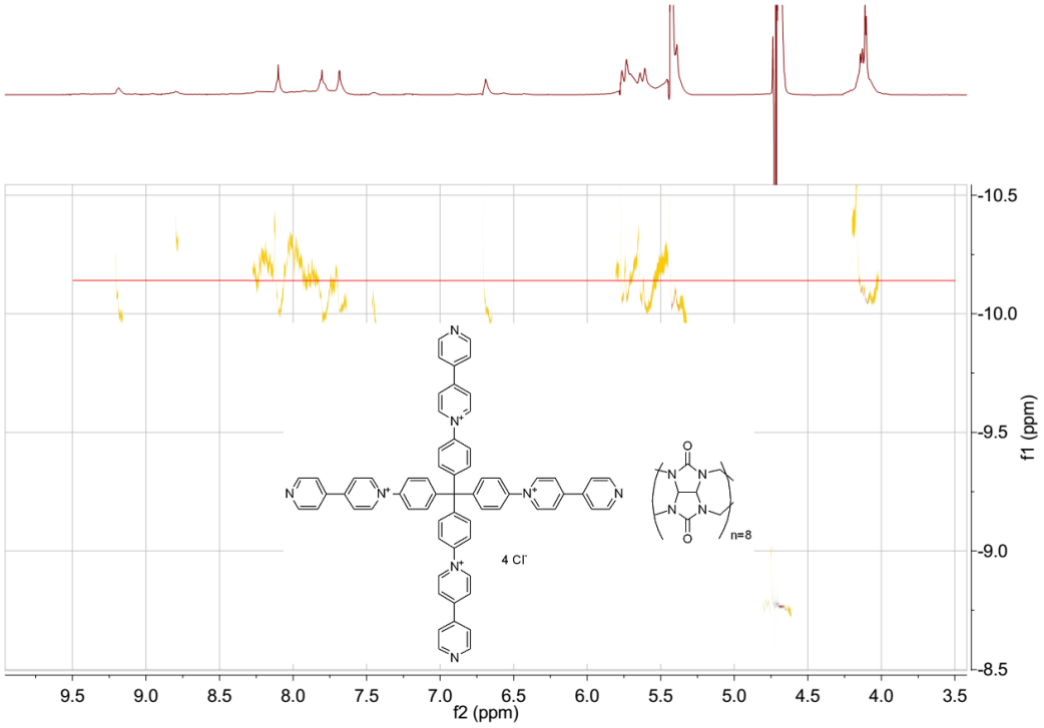

Figure S2. DOSY ^{1}H NMR spectrum (400 MHz) of the solution of **SOF-1** ([**1**] = 1.0 mM) in D_2O. The ordinate represents the log value of the diffusion constant.

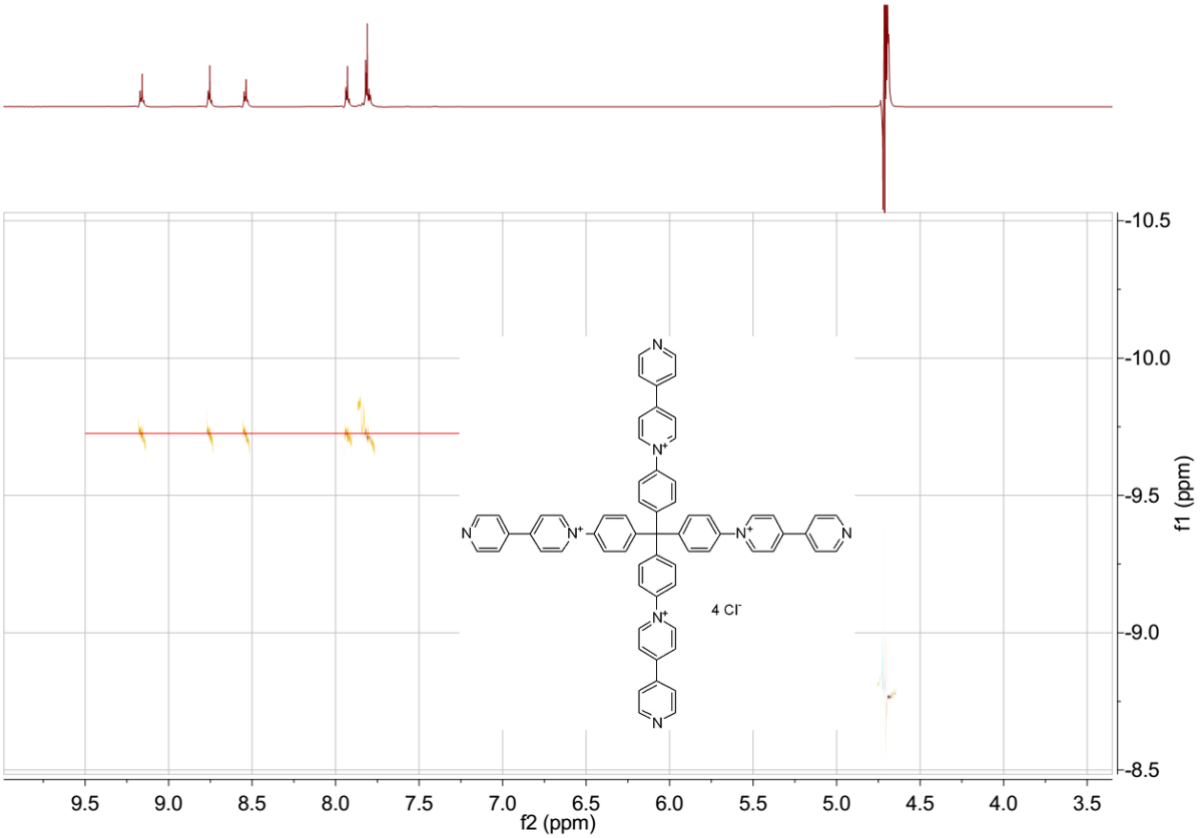

Figure S3. DOSY ^{1}H NMR spectrum (400 MHz) of the solution of **1** (1.0 mM) in D_2O. The ordinate represents the log value of the diffusion constant.

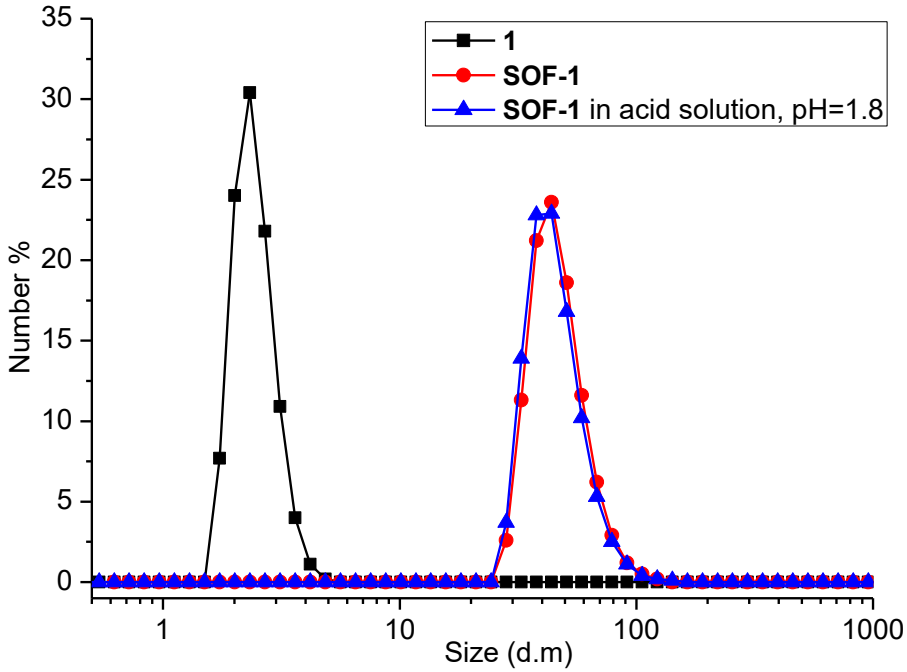

Figure S4. DLS profiles of the mixtures of molecule **1** and **SOF-1** made of **1** with CB[8] in water at 25 °C. The data represent the hydrodynamic diameters (D_H). [**1**] = 1.0 mM, CB[8] = 2.0 mM. The peak values of the solutions were originally afforded by the instrument.

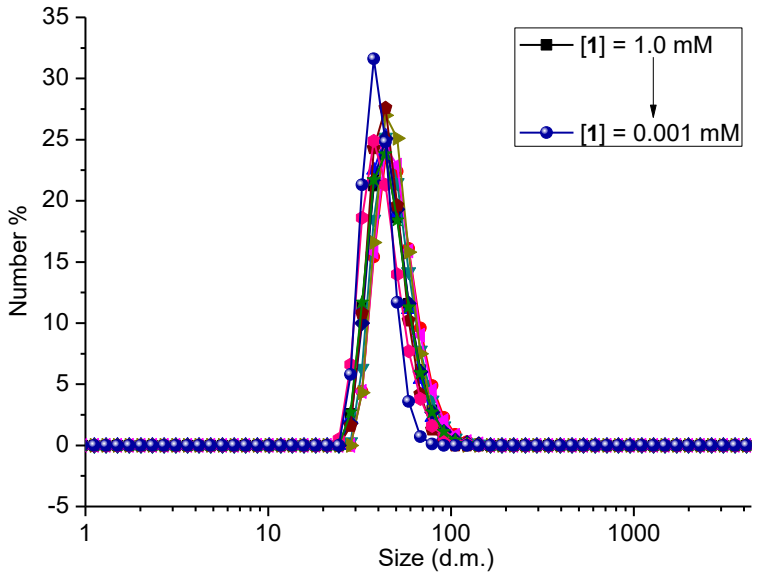

Figure S5. The of DLS result of SOF in water at 25 °C varied concentrations of [**1**] from 1.0 mM to 0.001 mM. The stable hydrodynamic diameters indicated the stability of **SOF-1** at different concentrations. All the samples were measued after being left to stand for 48 hours.

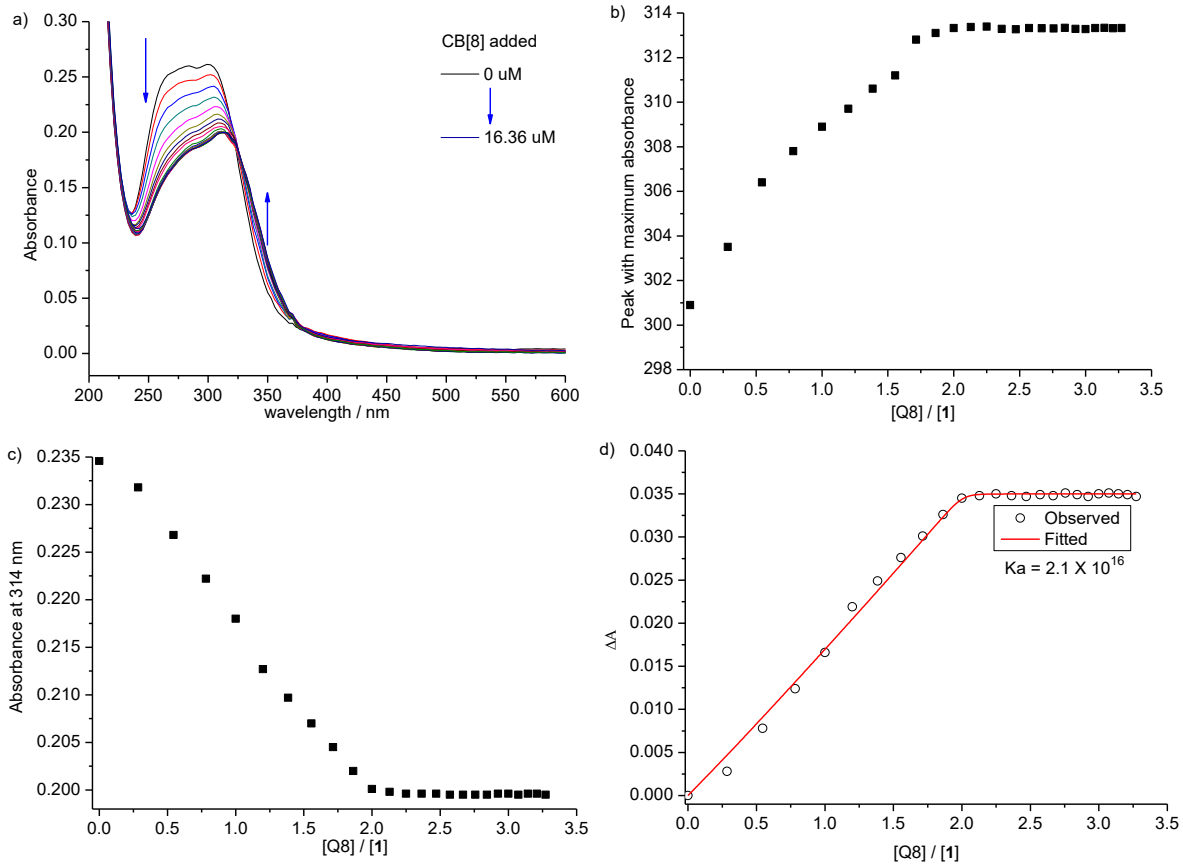

Figure S6. a) The UV-Vis titration spectrum, b) red shift, c) hypochromism at 314 nm of **1**, and d) the resulted absorbance change (dot) and fitted curve (red line) for apparent association constant (K_a) with the increasing of (CB[8], 0-16.36 μM) into fixed solution of **1** ([**1**] = 5 μM).

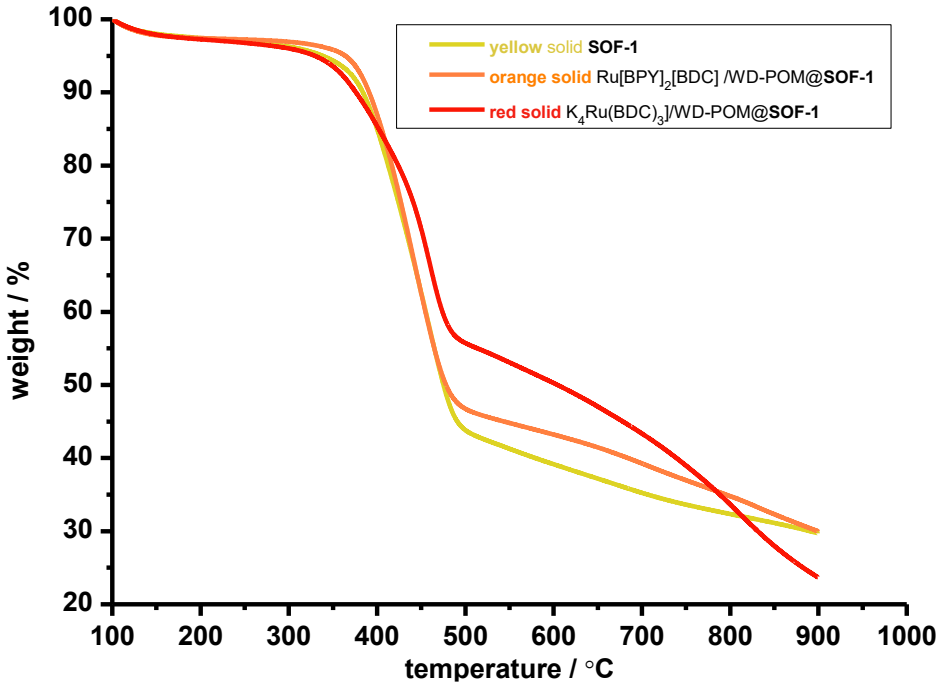

Figure S7. Thermogravimetric analysis of **SOF-1**, $K_4Ru(BDC)_3$/WD-POM@**SOF-1** and $Ru(BPY)_2(BDC)$/WD-POM@**SOF-1** that were obtained from slow evaporation, successive wash by methanol and water, and finally dried under vacuum.

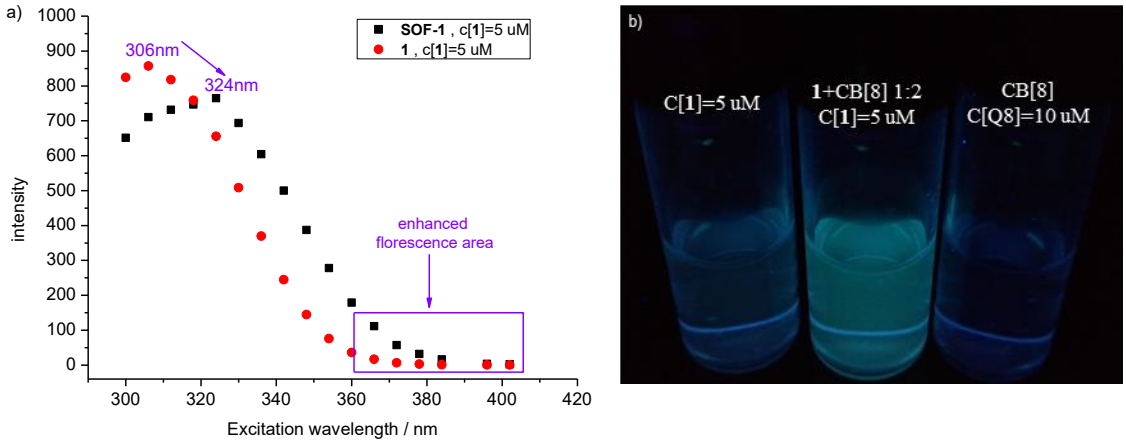

Figure S8. a) Enhanced fluorescence area of **SOF-1** (**1**:CB[8] = 1:2, c[**1**]=5 M) compared with **1**, and b) its image seen by naked eys under 365 nm light.

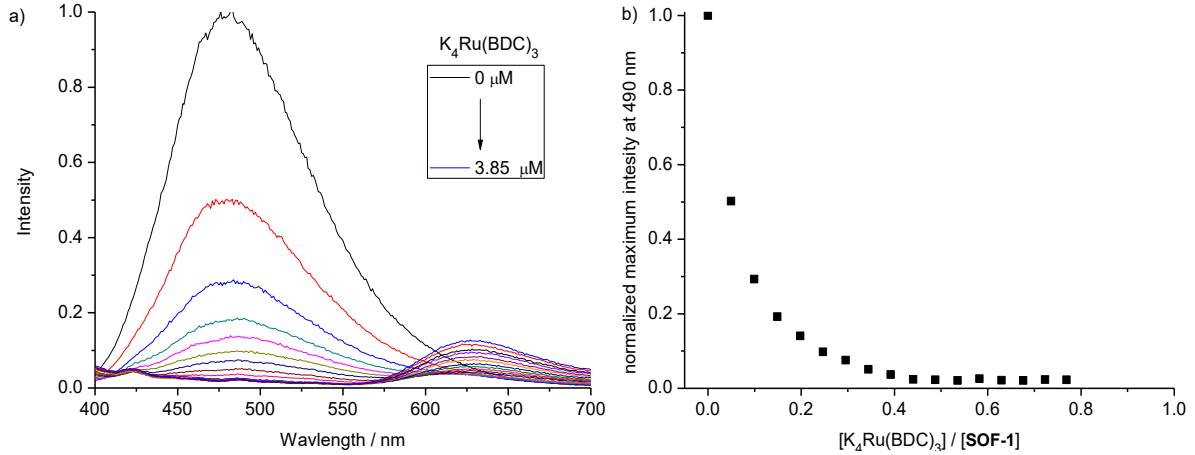

Figure S9. Fluorescence quenching of **SOF-1** ([**1**]=5 μM) at the excitation of 370 nm by adding guest $K_4Ru(BDC)_3$ (0-3.85 μM).

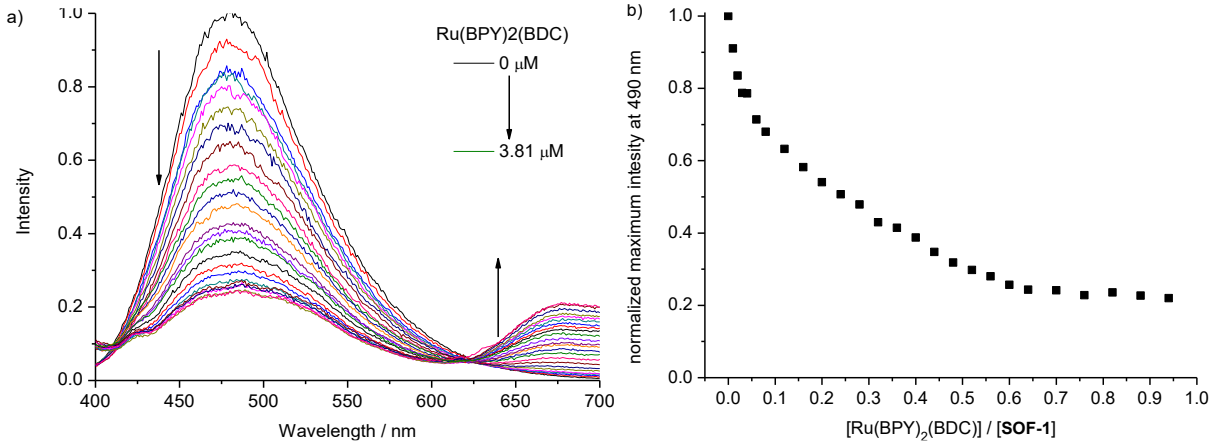

Figure S10. Fluorescence quenching of **SOF-1** ([**1**]=5 μM) at the excitation of 370 nm by adding guest $Ru(BPY)_2(BDC)$ (0-3.81μM).

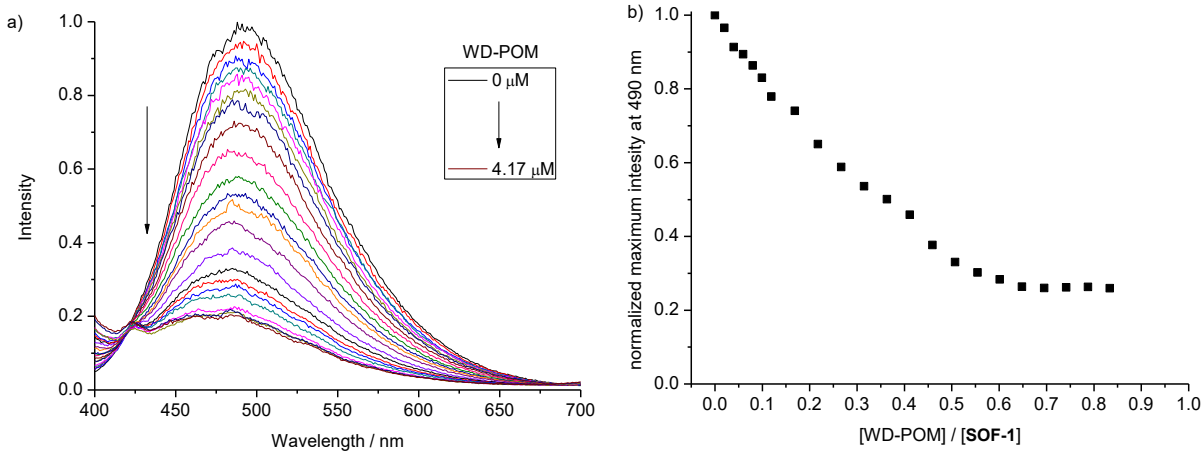

Figure S11. Fluorescence quenching of **SOF-1** ([**1**]=5 μM) at the excitation of 370 nm by adding guest WD-POM (0-4.17 μM).

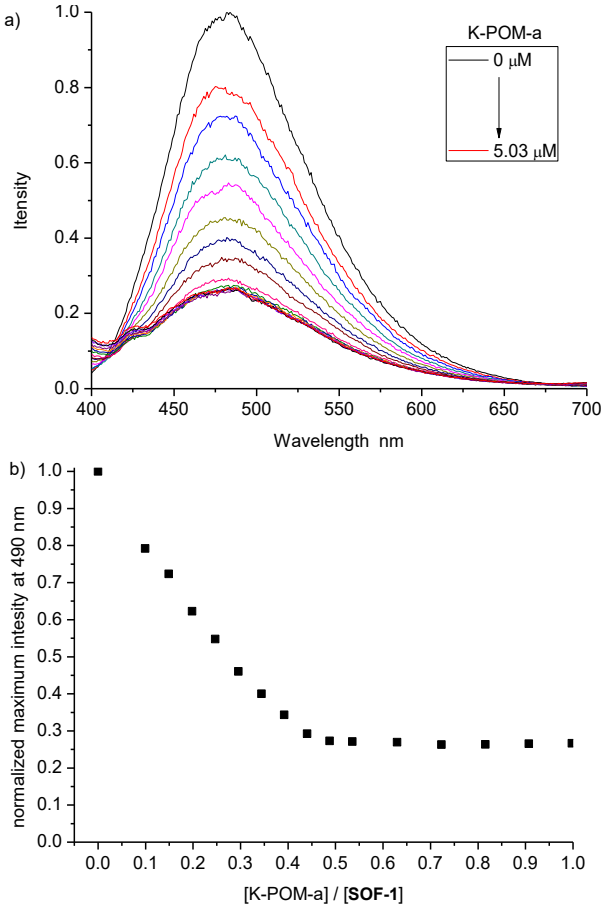

Figure S12. Fluorescence quenching of **SOF-1** ([**1**]=5 μM) at the excitation of 370 nm by adding guest K-POM-a (0-5.03 μM).

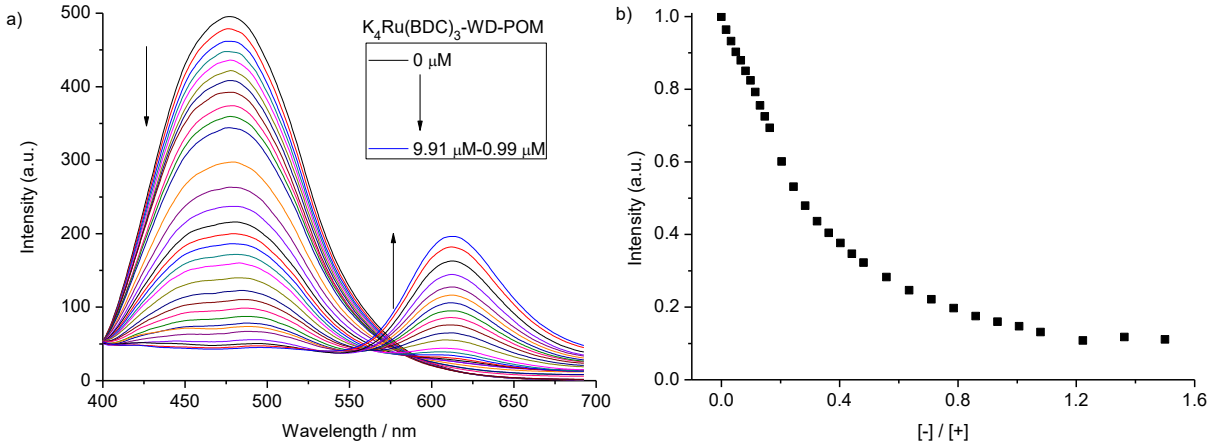

Figure S13. Fluorescence quenching of **SOF-1** ([**1**]=5 μM) at the excitation of 370 nm by adding guest $K_4Ru(BDC)_3$/WD-POM (0-9.91/0.99 μM).

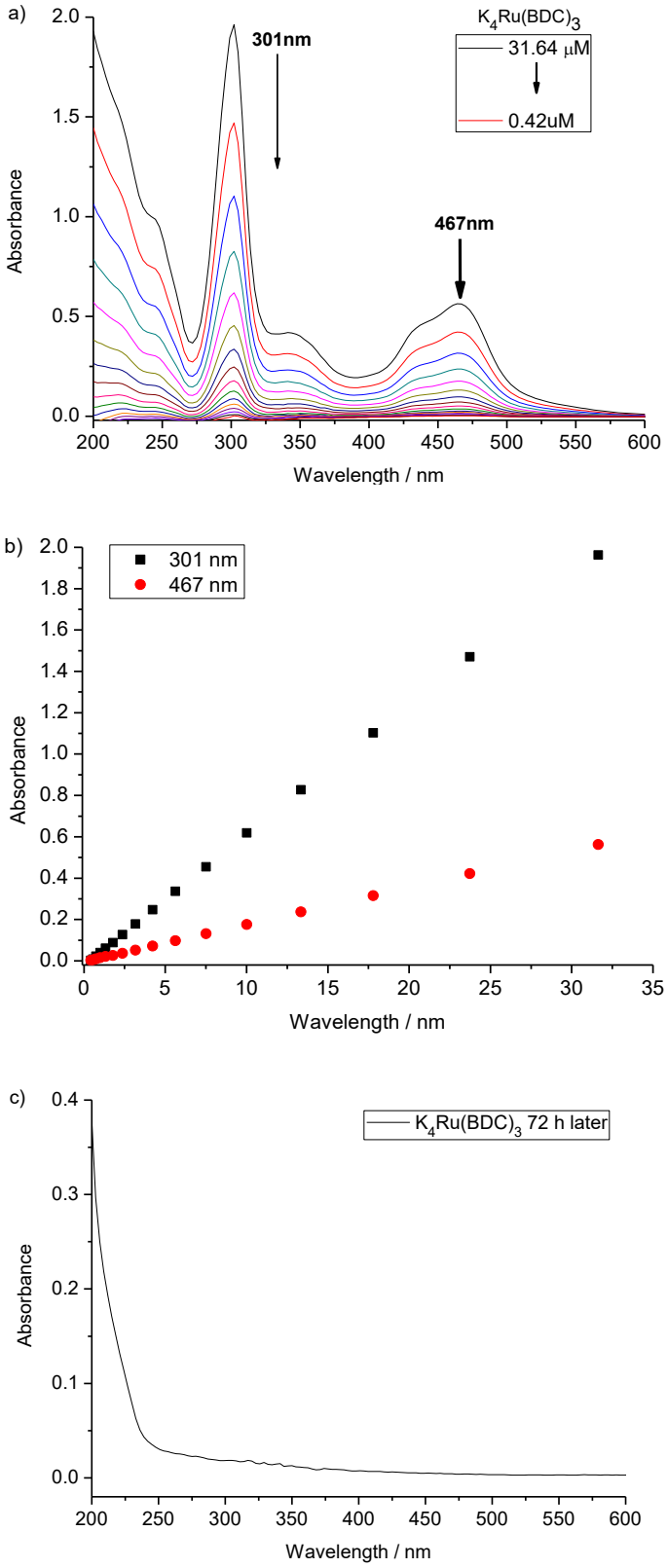

Figure S14. a) UV-Vis spectrum by gradually dilution, b) the plots of the absorbance of guest $K_4Ru(BDC)_3$, c) and the possible leaching of guest $K_4Ru(BDC)_3$ from the $K_4Ru(BDC)_3$ @**SOF-1** hybrid after dialysis for 72h in water. The results indicated that the guest was absorbed by **SOF-1** without leaching from the self-assembly hybrid.

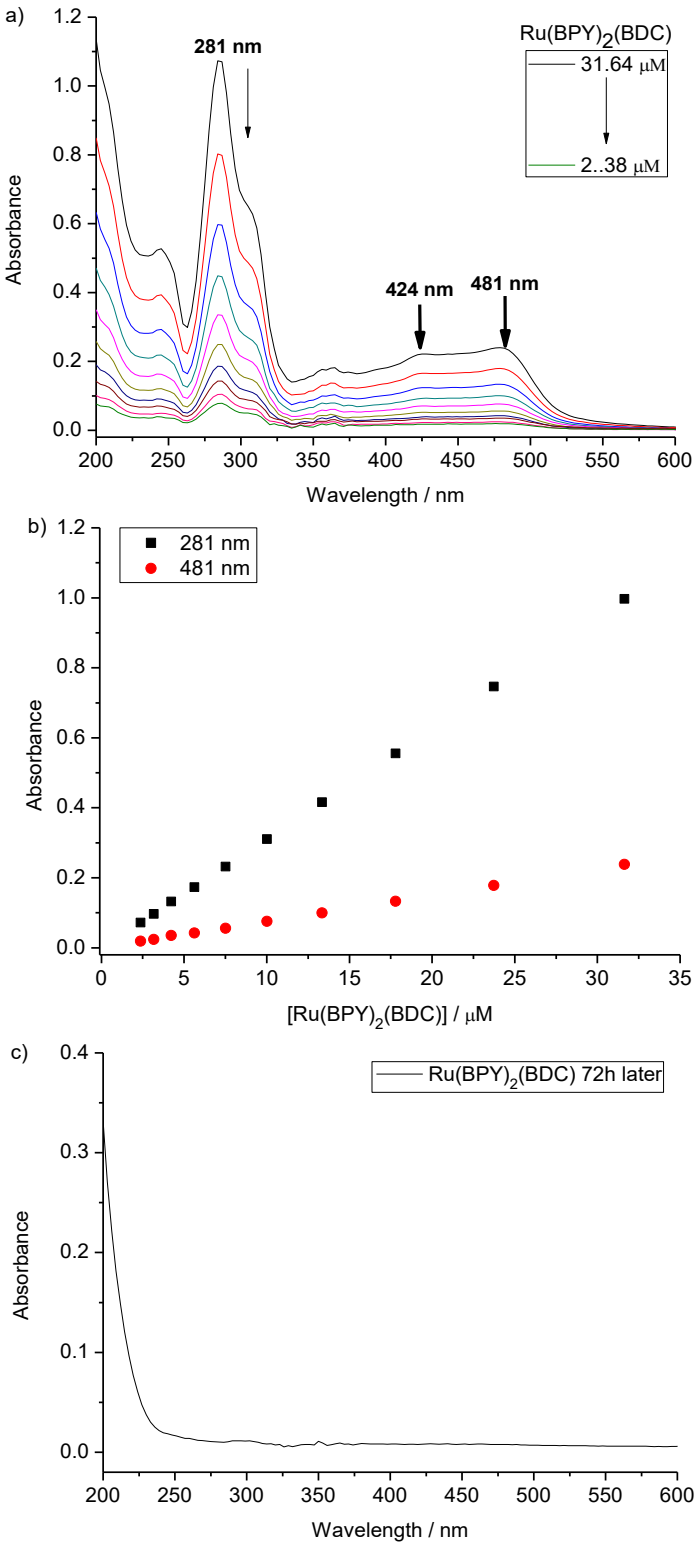

Figure S15. a) UV-Vis spectrum by gradually dilution, b) and the plots of the absorbance of guest $Ru(BPY)_2(BDC)$, c) the possible leaching of guest $Ru(BPY)_2(BDC)$ from the $Ru(BPY)_2(BDC)$@**SOF-1** hybrid after dialysis for 72h in water. The results indicated that the guest was absorbed by **SOF-1** without leaching from the self-assembly hybrid.

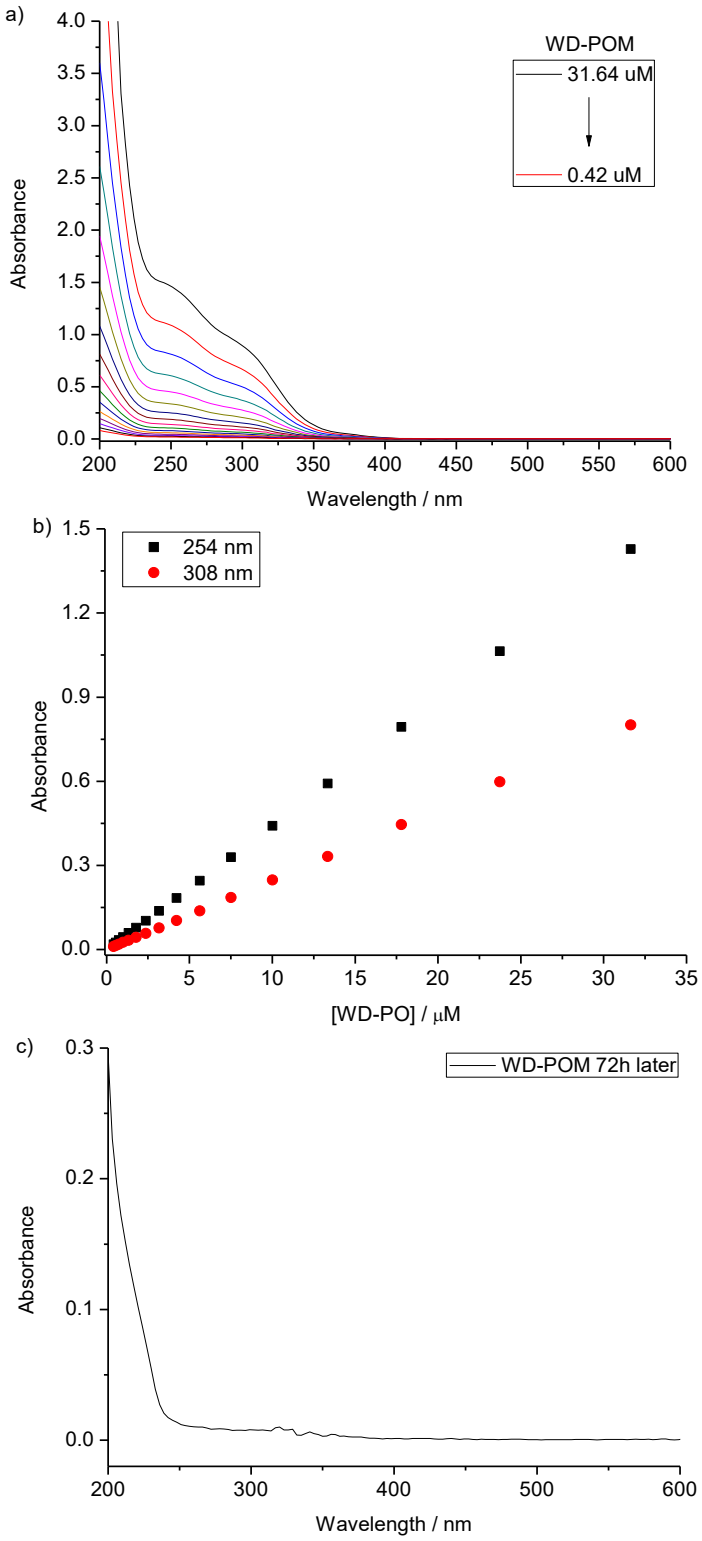

Figure S16. a) UV-Vis spectrum by gradually dilution, b) and the plots of the absorbance of guests WD-POM, c) the possible leaching of guests WD-POM from the WD-POM@**SOF-1** hybrid after dialysis for 72h in water. The results indicated that the guest was absorbed by **SOF-1** without leaching from the self-assembly hybrid.

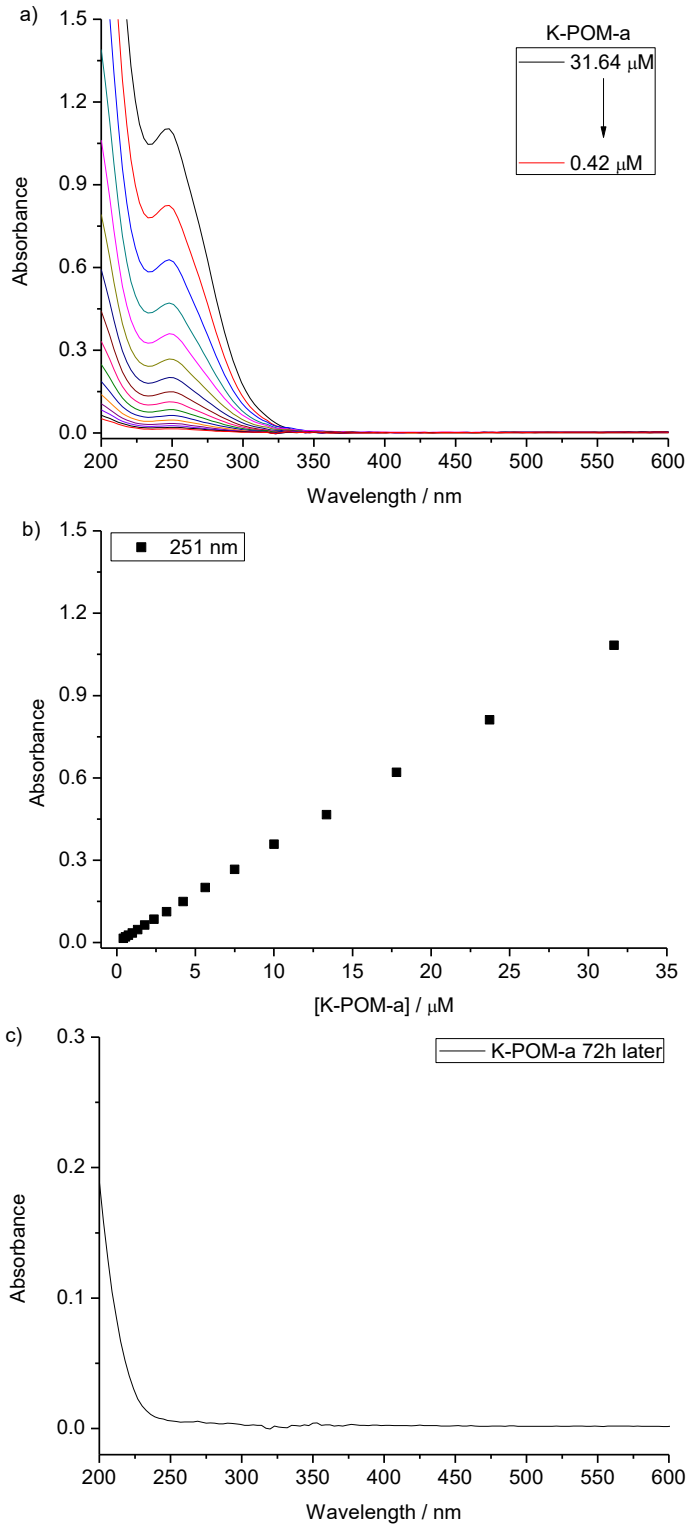

Figure S17. a) UV-Vis spectrum by gradually dilution, b) the plots of the absorbance of guests K-POM-a, c) the possible leaching of guests K-POM-a from the K-POM-a @**SOF-1** hybrid after dialysis for 72h in water. The results indicated that the guest was absorbed by **SOF-1** without leaching from the self-assembly hybrid.

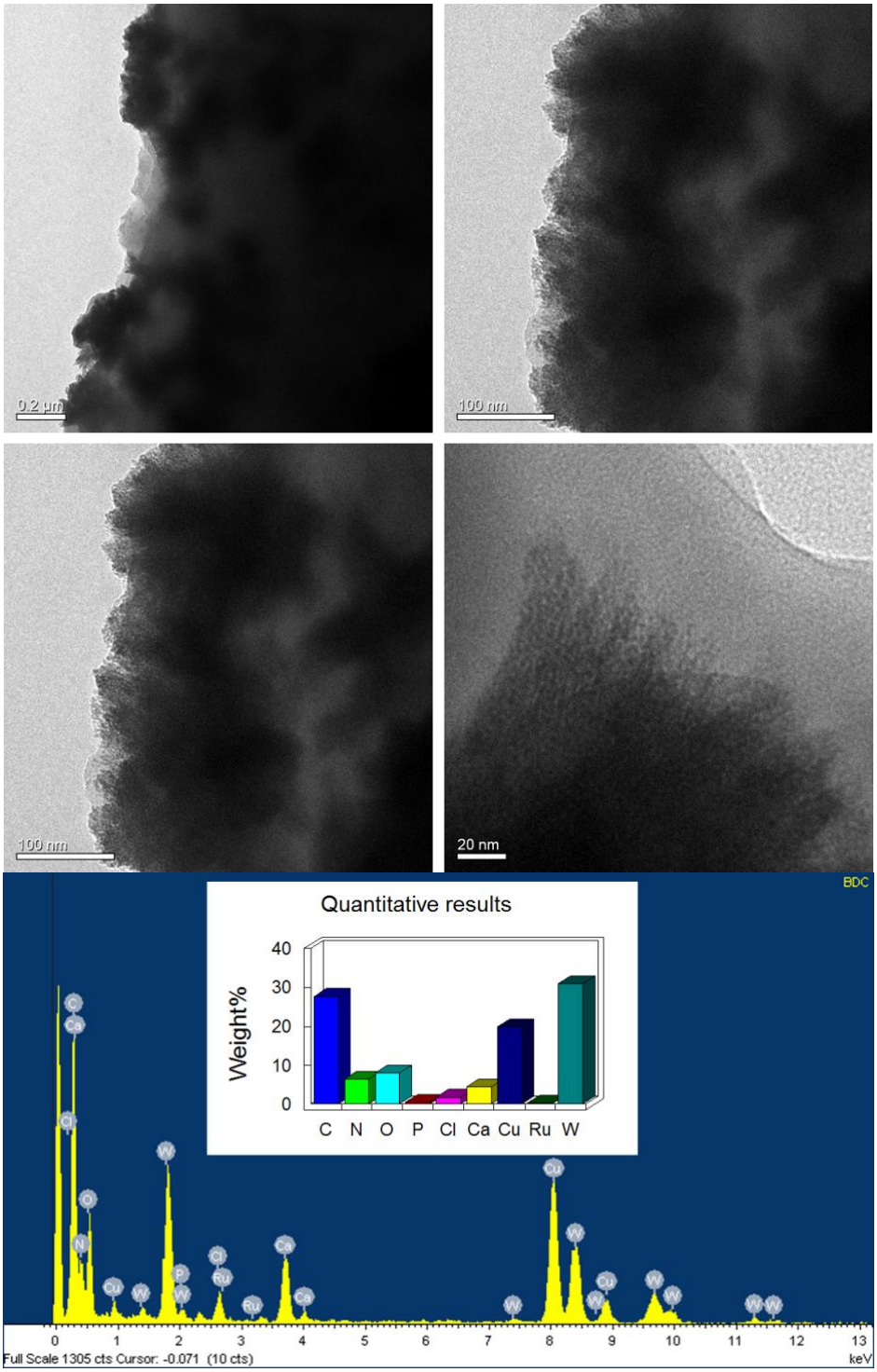

Figure S18. TEM images of $K_4Ru(BDC)_3$/WD-POM@**SOF-1** exhibit a uniform crystalline clusters (upper) and EDX results (down) indicated the content of the hybrid.

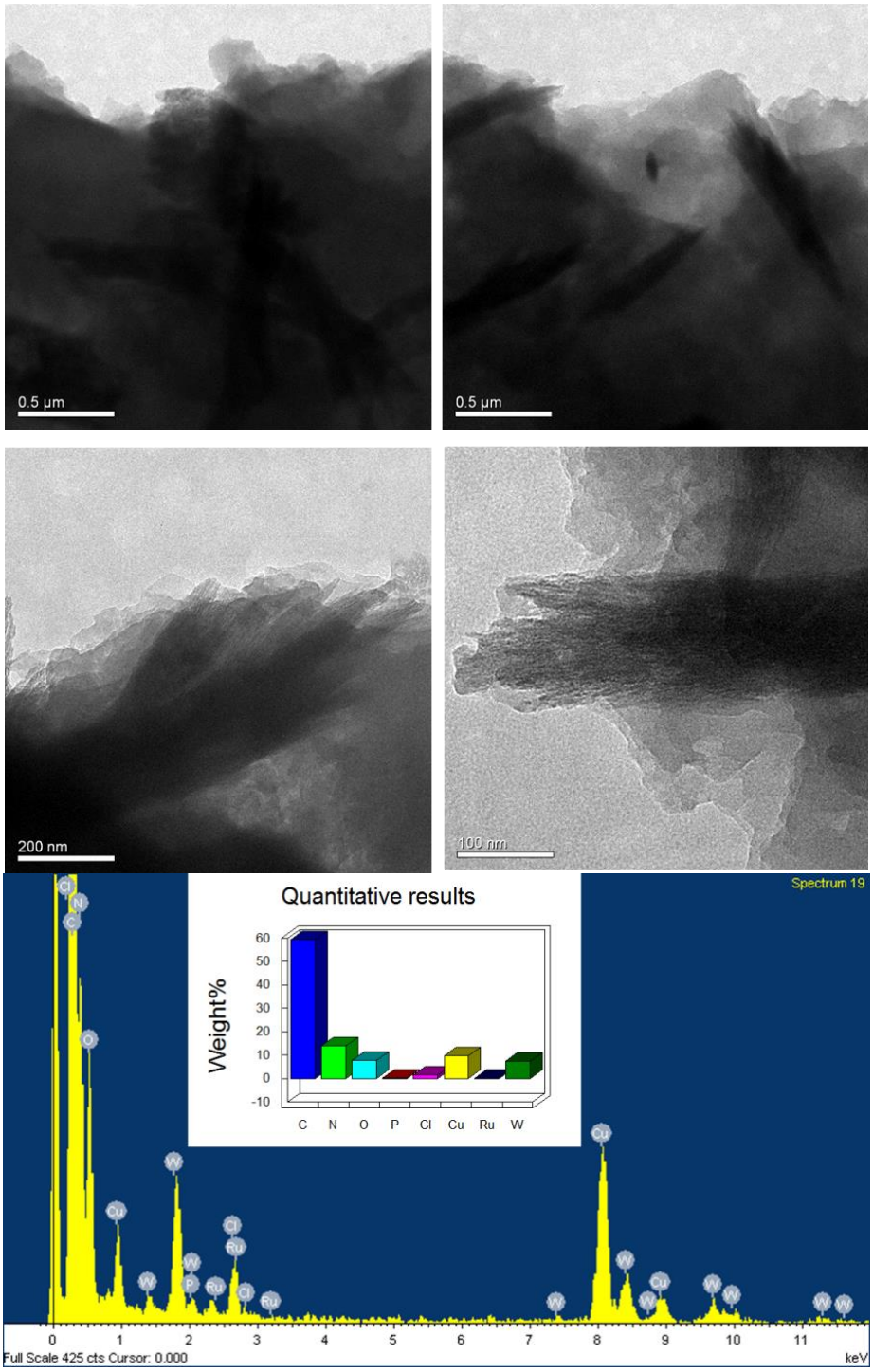

Figure S19. TEM images of $Ru(BPY)_2(BDC)$/WD-POM@**SOF-1** exhibit a uniform crystalline clusters (upper) and EDX results (down) indicated the content of the hybrid.

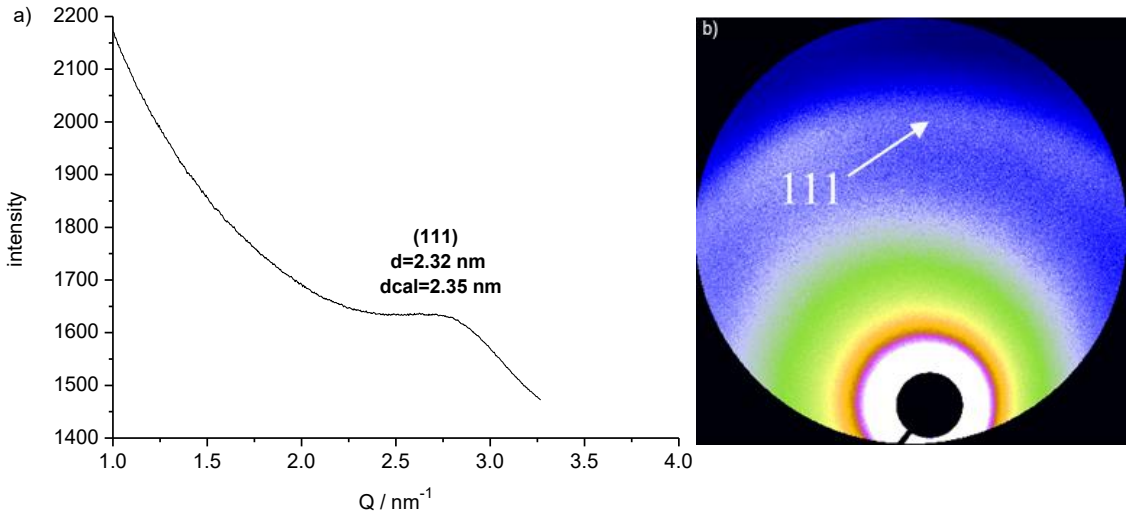

Figure S20. a) Synchrotron SAXS profile, and b) 2D image of $K_4Ru(BDC)_3$/K-POM-a@**SOF-1** powder crystals.

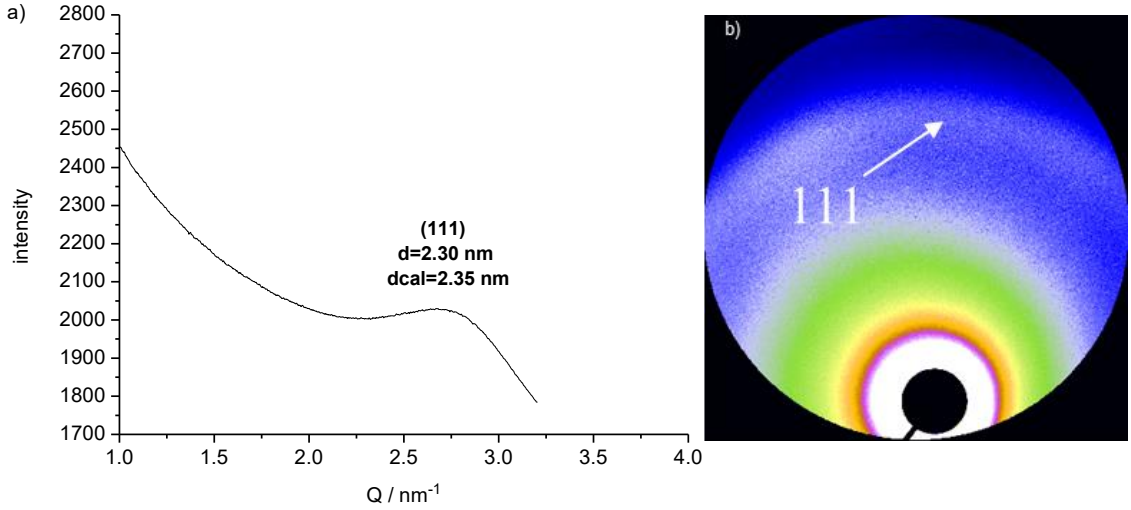

Figure S21. a) Synchrotron SAXS profile, and b) 2D image of $Ru(BPY)_2(BDC)$/WD-POM@**SOF-1** powder crystals.

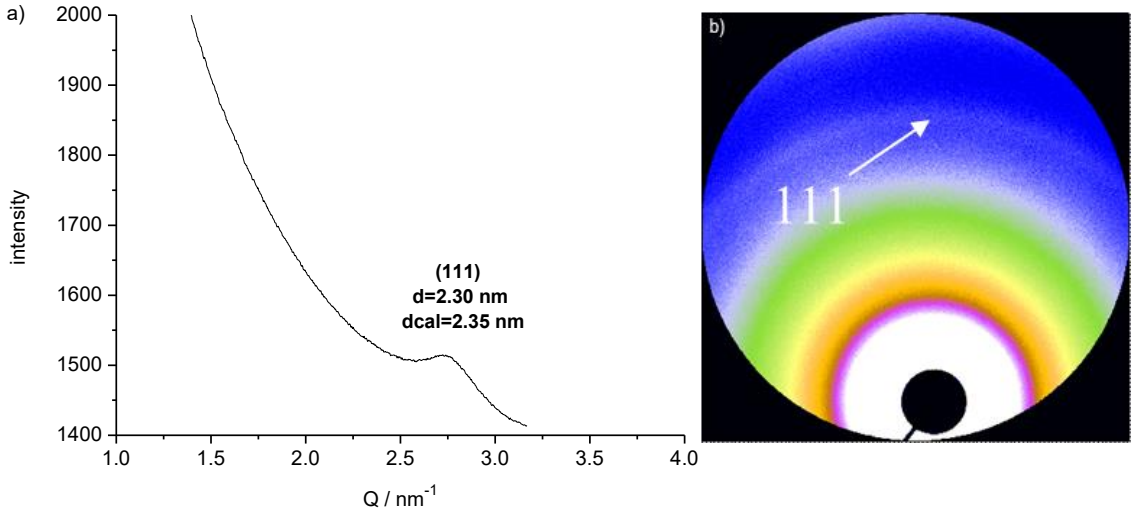

Figure S22. a) Synchrotron SAXS profile and b) 2D image of $Ru(BPY)_2(BDC)$/K-POM-a@**SOF-1** powder crystals.

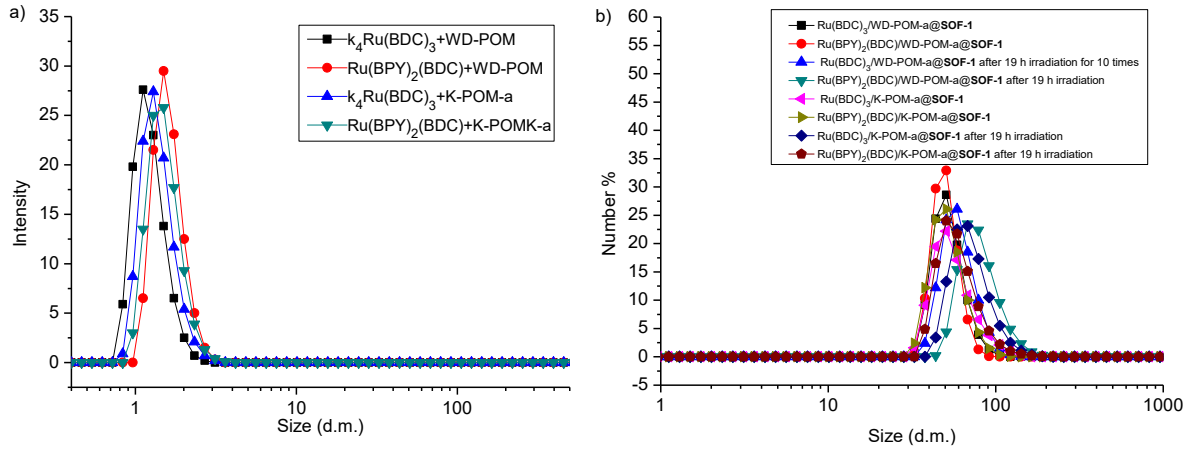

Figure S23. The of DLS profiles of a) different photosensitizers/catalysts mixtures and b) photosensitizers/catalysts@**SOF-1** hybrids before and after irradiation for 19 h in acid aqueous solution (pH=1.8) at 25 °C with concentration of photosensitizers to be 2 μM, catalysts to be 20 μM, ,and SOF to be 50 μM, respectively.

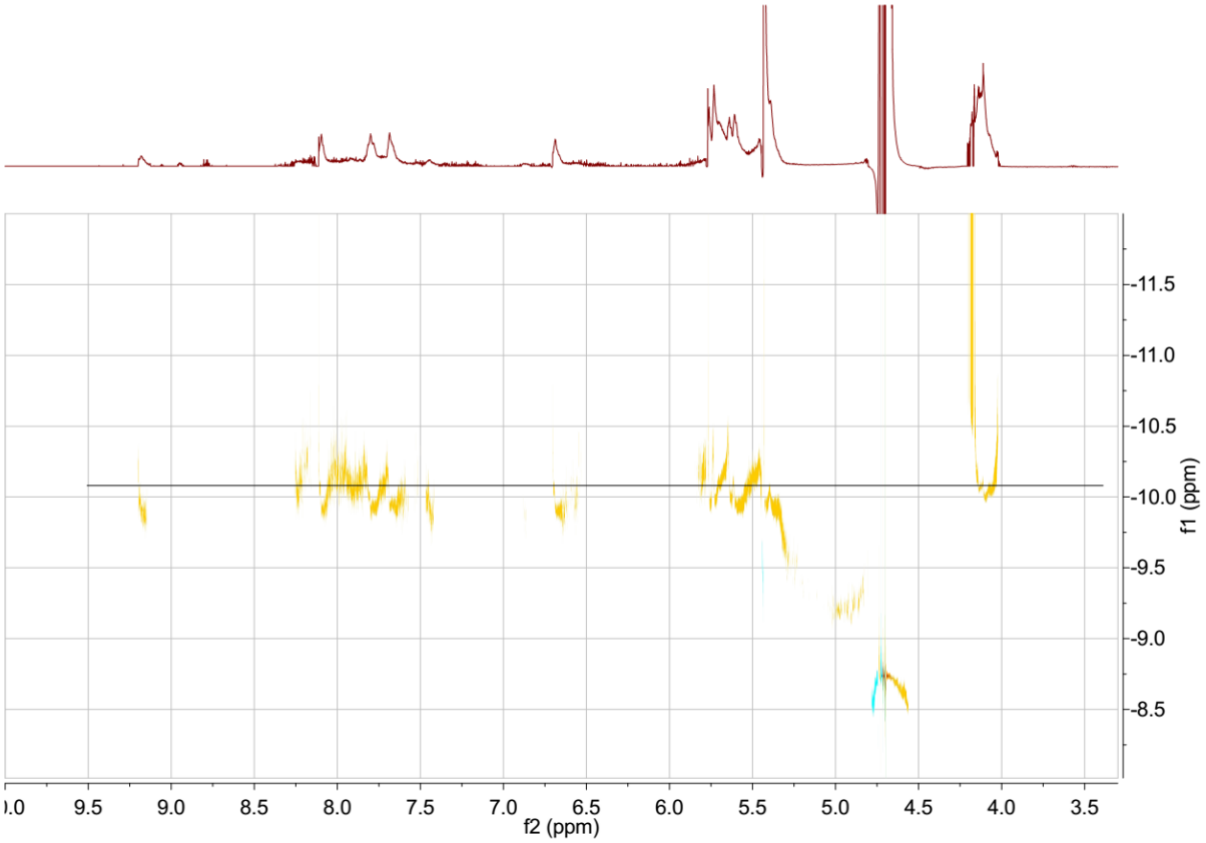

Figure S24. DOSY ^{1}H NMR spectrum (400 MHz) of the mixture of **SOF-1** ([**1**]=1.0 mM), $K_4Ru[BDC]_3$ (0.2 mM) and WD-POM (0.02 mM) in D_2O showed similar peaks with a series of noise which be attributed to the adding of $K_4Ru(BDC)_3$ and WD-POM. The ordinate represents the log value of the diffusion constant. Note： this spectrum was obtained from the former sample by adding $K_4Ru(BDC)_3$ and WD-POM.

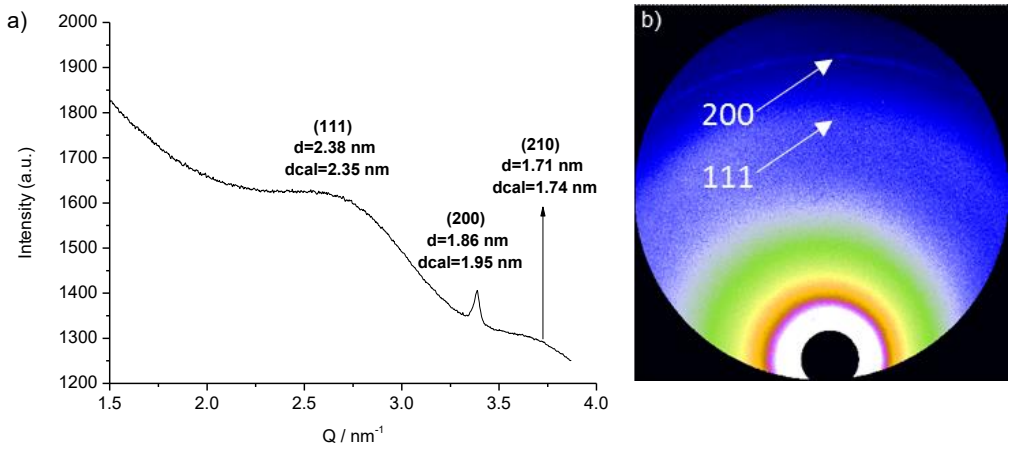

Figure S25. a) Synchrotron SAXS profile and b) 2D image of $K_4Ru(BDC)_3$@**SOF-1** powder crystals.

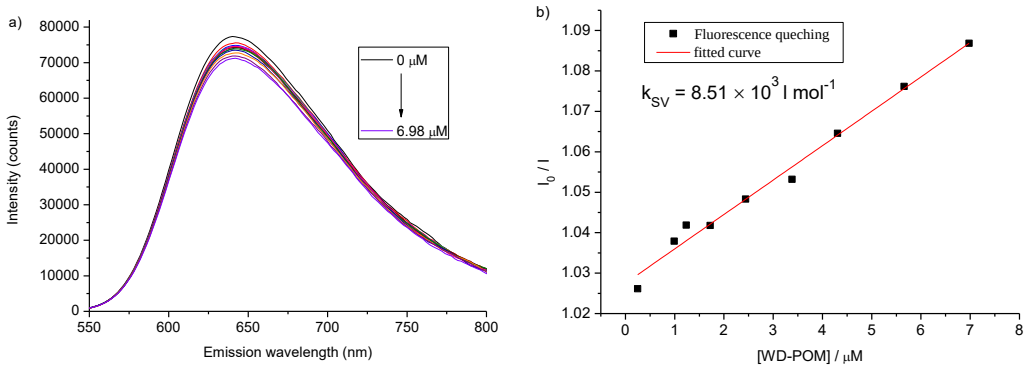

Figure S26. a) Steady-state emission quenching of $K_4Ru(BDC)_3$ (20 μM) by adding WD-POM (0-6.98 μM) in the absence of **SOF-1** with λ_{ex} = 460 nm, λ_{em} = 627 nm, b) and the corresponding quenching constants (k_{SV}) fitted by Stern-Volmer equation (red line). Conditions: $K_4Ru(BDC)_3$ (20 μM), MeOH (20 % v/v), pH = 1.8, WD-POM (2 μM).

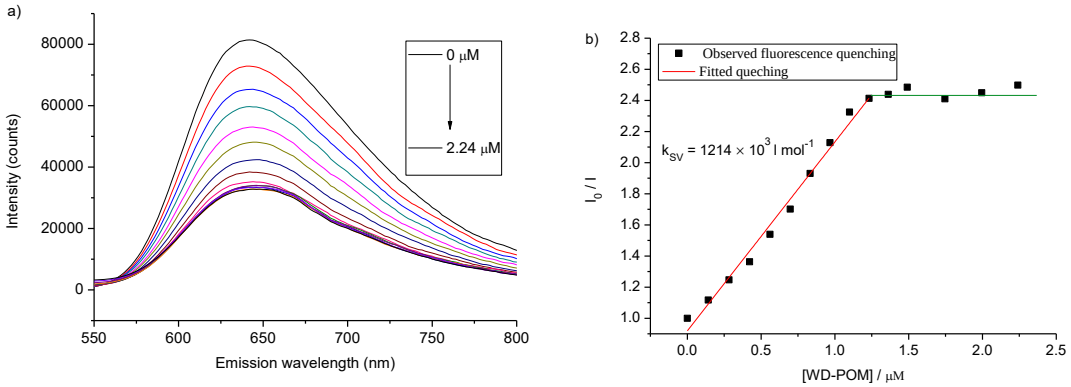

Figure S27. a) Steady-state emission quenching of $K_4Ru(BDC)_3$ (20 μM) by adding WD-POM (0-2.24 μM) in the presence of **SOF-1** ([**1**] = 50 μM**)** with λ_{ex} = 460 nm, λ_{em} = 627 nm, b) and the corresponding quenching constants (k_{SV}) fitted by Stern-Volmer equation (red line). Conditions: $K_4Ru(BDC)_3$ (20 μM), MeOH (20 % v/v), pH = 1.8, WD-POM (2 μM).

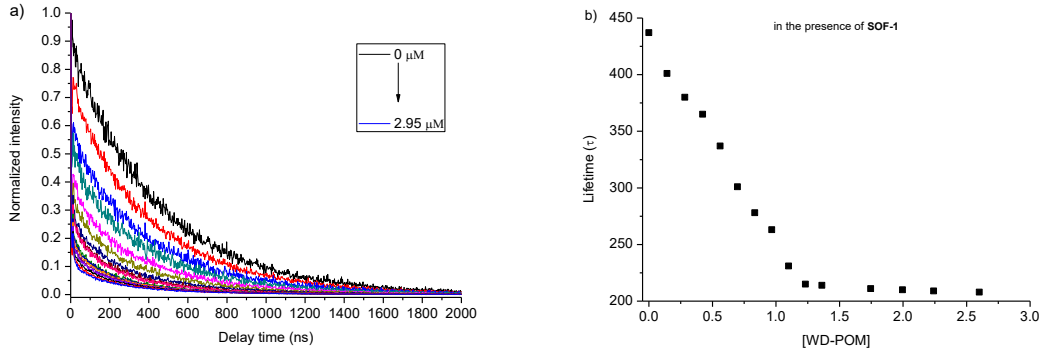

Figure S28. a) Decay transients measured at 627 nm (λ_{ex} = 375 nm), b) and their corresponding fitted lifetime by adding WD-POM (0-2.24 µM) in the presence of **SOF-1** ([**1**] = 50 µM**)**. Conditions: $K_4Ru(BDC)_3$ (20 µM), MeOH (20 % v/v), pH = 1.8, WD-POM (2 µM).

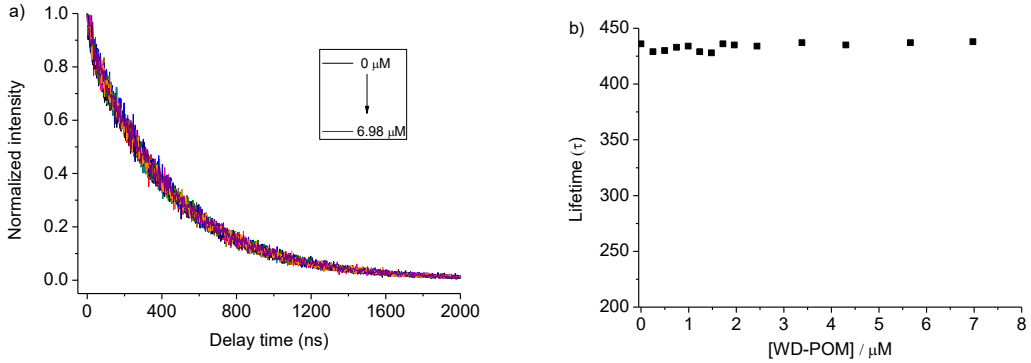

Figure S29. a) Decay transients measured at 627 nm (λ_{ex} = 375 nm), b) and their corresponding fitted lifetime by adding WD-POM (0-6.98 µM) in the absence of **SOF-1**. Conditions: $K_4Ru(BDC)_3$ (20 µM), MeOH (20 % v/v), pH = 1.8, WD-POM (2 µM).

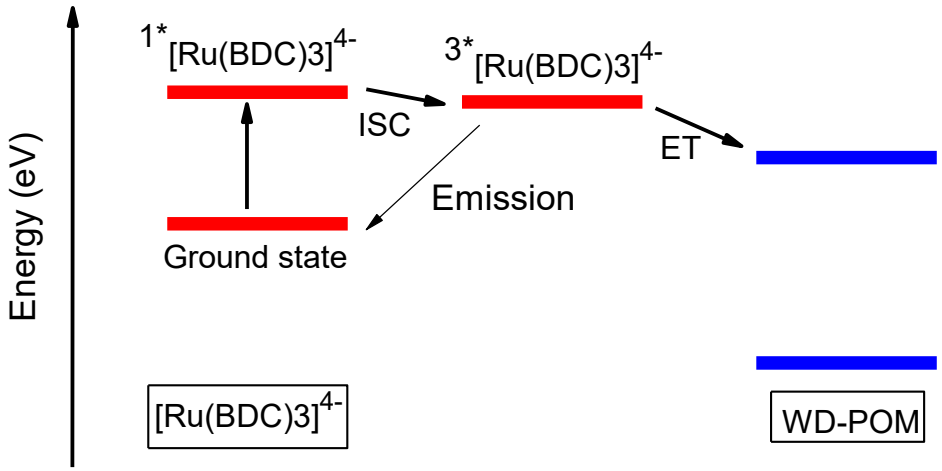

Figure S30. Energy level diagram for $[Ru(BDC)_3]_{4-}$ and WD-POM in the presence of **SOF-1**. $[Ru(BDC)_3]_{4-}$ absorbs photon generating the singlet excited-state $^{1*}[Ru(BDC)_3]_{4-}$ which efficiently transfer to the triplet state $^{3*}[Ru(BDC)_3]_{4-}$ by inter-system crossing (ISC). The triplet state decay to the ground state is in competition with two other processes: emission or electron transfer (ET) to the LUMO of the WD-POM which enables the hydronium reduction.

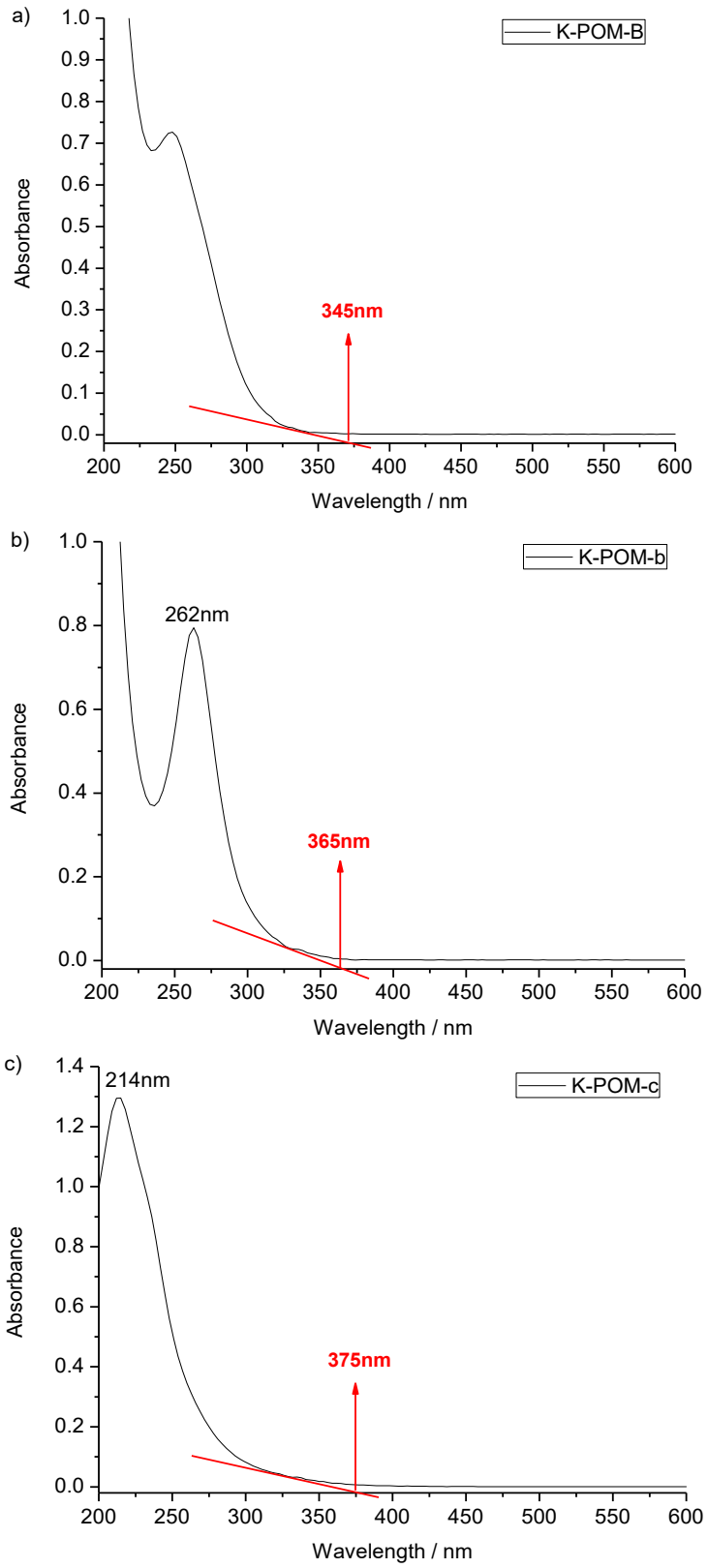

Figure S31. UV-Vis of a) K-POM-a, b) K-POM-b, and c) K-POM-c in water at the concentration of 20 uM at room temperature, which were used to caculated the band gap of the above three photosensitizers to be 3.59, 3.31 and 3.30 eV.

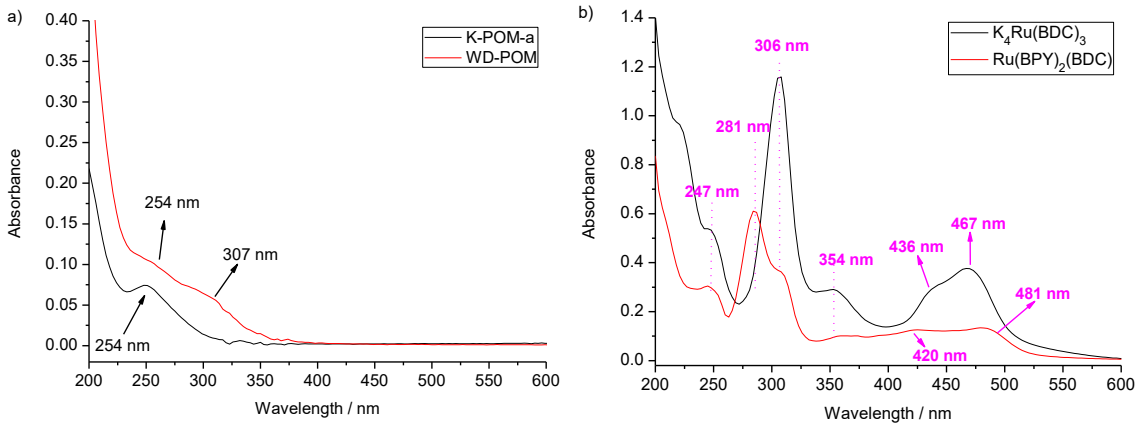

Figure S32. UV-Vis spectrum of the WD-POM and K-POM-a (2 μM), and b) $K_4Ru(BDC)_3$ and $Ru(BPY)_2(BDC)$ (20 μM) in water.

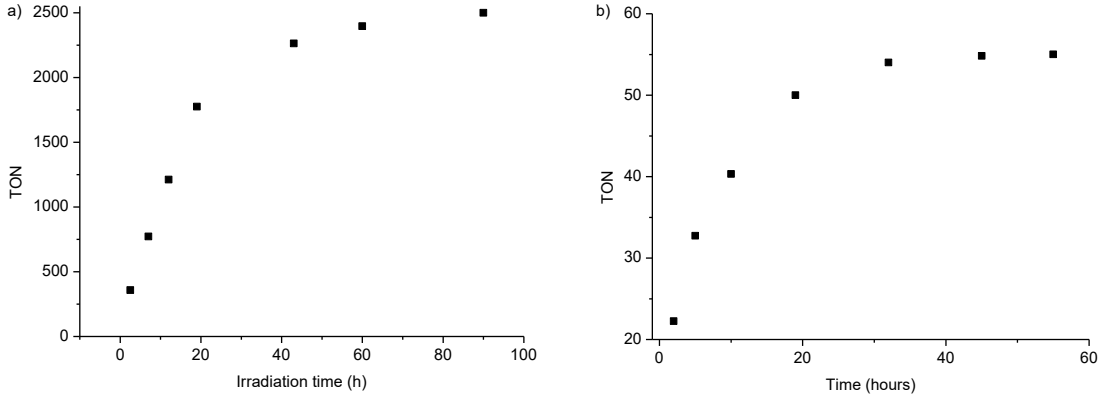

Figure S33. TON values of the H_2 generation systems vs irradiation time a) in the presence and b) absence of **SOF-1** ([**1**] = 50 μM) versus the irradiation time. The reaction system contained photosensitizer $[Ru(BDC)_3]_{4-}$ (20 μM), catalyst WD-POM (2 μM), methanol (20 %, v/v) and pH = 1.8.

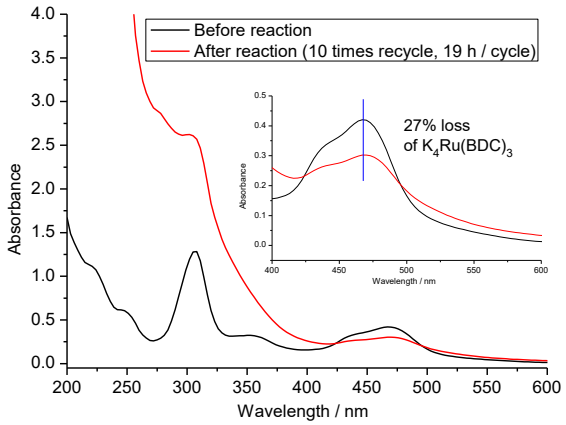

Figure S34. UV-vis spectrum of the reaction solution before and after 10-time recycled irradiation (19 h). The reaction system contained photosensitizer $[Ru(BDC)_3]_{4-}$ (20 μM), catalyst WD-POM (2 μM), methanol (20 %, v/v), **SOF-1** ([1] = 50 μM), and pH = 1.8.